

**Record Number:** 17900  
**Author, Monographic:** Fortin, J. P.//Bernier, M.//El Battay, A.//Gauthier, Y.  
**Author Role:**  
**Title, Monographic:** Estimation of surface variables at the sub-pixel level for use as input to climate and hydrological models  
**Translated Title:**  
**Reprint Status:**  
**Edition:**  
**Author, Subsidiary:**  
**Author Role:**  
**Place of Publication:** Québec  
**Publisher Name:** INRS-Eau  
**Date of Publication:** 2000  
**Original Publication Date:** Mars 2000  
**Volume Identification:**  
**Extent of Work:** vii, 59  
**Packaging Method:** pages  
**Series Editor:**  
**Series Editor Role:**  
**Series Title:** INRS-Eau, rapport de recherche  
**Series Volume ID:** 564  
**Location/URL:**  
**ISBN:** 2-89146-324-2  
**Notes:** Rapport annuel 1999-2000  
**Abstract:**  
**Call Number:** R000564  
**Keywords:** rapport / ok/ dl

**ESTIMATION OF SURFACE VARIABLES AT THE SUB-PIXEL LEVEL FOR USE  
AS INPUT TO CLIMATE AND HYDROLOGICAL MODELS**

Final Report  
(post-launch phase)

to

**Centre national d'Études spatiales**

by

Jean-Pierre Fortin  
Monique Bernier  
Ali El Battay  
Yves Gauthier

Institut national de la recherche scientifique, INRS-Eau  
2800, rue Einstein, Case postale 7500, SAINTE-FOY (Québec), G1V 4C7

Rapport de recherche No R- 564

Mars 2000

© INRS-Eau 2000

ISBN 2-89146-3242

# TABLE OF CONTENT

1	INTRODUCTION .....	1
2	OBJECTIVES OF THE INVESTIGATION .....	3
3	APPROACH USED DURING THE PRE-LAUNCH PHASE OF INVESTIGATION .....	5
3.1	Simulation of SPOT-4 HRVIR and VGT images .....	5
3.1.1	Introduction.....	5
3.1.2	Simulation of HRVIR and VGT data.....	7
3.2	Processing of simulated VGT data for estimation of the mean reflectances of land use classes in a specific geographical area.....	7
3.2.1	Chosen approach assuming perfect registration of the images .....	7
3.2.2	Estimation of the co-location accuracy in an operational context.....	8
3.3	Processing of simulated VGT data for the estimation of the percentages of snow cover present in each broad land use class of any VGT pixel in a specific geographical area.....	10
3.3.1	The spectral mixture approach in the case of a VGT image with partial snow cover .....	10
3.3.2	Description of the chosen approach .....	12
4	MAIN RESULTS OBTAINED DURING THE PRE-LAUNCH PHASE OF THE INVESTIGATION .....	13
4.1	Determination of the actual position of a VGT image relative to its expected position .....	13
4.2	Determination of the reflectances of the land use classes .....	14
4.3	Determination of the snow cover percentages at the sub-pixel level .....	17
4.3.1	Main characteristics of the HRVIR and VGT images.....	17
4.3.2	Sub-pixel estimation of snow cover.....	17
5	ACQUISITION OF VGT AND HRVIR IMAGES DURING THE POST-LAUNCH PHASE OF THE INVESTIGATION .....	25
5.1	Spatio-temporal evolution of the snow cover in Southern Québec during the 1998-1999 winter .....	25
5.2	VGT and HRVIR images pre-selected for the investigation.....	27
6	PROCESSING OF THE ACTUAL VEGETATION AND HRVIR IMAGES.....	29
6.1	Atmospheric corrections .....	29
6.2	Geometric corrections.....	30
6.2.1	HRVIR and HRV images.....	30
6.2.2	VEGETATION images.....	30
6.2.3	Relative location of the VEGETATION images between themselves and with respect to the HRVIR images.....	30
6.3	Estimation of land use reflectances.....	35
6.4	Estimation of snow cover at the sub-pixel level .....	35
6.4.1	Selection of VEGETATION and high resolution images (HRVIR and HRV).....	35
6.4.2	Analysis of the VEGETATION and HRVIR images taken on April 11, 1999.....	38
6.4.3	Analysis of the VEGETATION and HRV images taken on April 2, 1999.....	43
6.4.4	Mapping of the snow cover at the sub-pixel level .....	47
6.4.5	Mapping of the snow cover at the sub-pixel level for a larger area in Southern Québec.....	50
7	DISCUSSION.....	55
8	CONCLUSION.....	57
	BIBLIOGRAPHY.....	59



## LIST OF TABLES

Table 4.1	Estimated land use reflectances from the VGT spectral bands vs HRVIR reflectances, at location (0,0) for the August 28 <sup>th</sup> 1995 simulated images. ....	15
Table 4.2	Mean reflectances (standard deviation) and percentage of occupation of each identified land use classes on the spring image (April 2, 1988).....	18
Table 5.1	Acquisition of SPOT images in 1999 .....	28
Table 6.1	Multispectral and multitemporal registration of VGT images with respect to the HRVIR image taken on April 11, 1999. ....	32
Table 6.2	Comparison of reflectance values estimated from HRVIR and VGT pixels . Only land use classes in bold are used in figure 6.3 .....	36



## LIST OF FIGURES

Figure 3.1	Areas covered by each of the three images used in the project (A) Nicolet - Trois-Rivières region (B) Southern Quebec, between the St-François and the Chaudière rivers; (C) St-François watershed.....	6
Figure 4.1	VGT estimated reflectances VS HRVIR reflectances.....	16
Figure 4.2	Snow cover estimations on VGT pixels.....	20
Figure 4.3	Snow cover estimation – April 2, 1988.....	22
Figure 5.1	Snow cover in Southern Québec from February to May 1999.....	26
Figure 6.1	Standard deviation mapping for the May 2, 1999. VGT spectral band B2.....	33
Figure 6.2	Multispectral and multitemporal registration of VGT images, with respect to the HRVIR image taken on April 11, 1999. □ is expected co-location error between VGT and HRVIR images.....	34
Figure 6.3	Comparison of land use reflectances as estimated from HRVIR and VGT pixels, for the images taken simultaneously on April 11, 1999 and spectral bands B2, B3 and B4.....	37
Figure 6.4	VGT images used as references.....	39
Figure 6.5	HRVIR and VGT images taken simultaneously on April 11, 1999.....	40
Figure 6.6	VGT and HRV images taken on April 2, 1999.....	41
Figure 6.7	Snow cover estimations with the F and SNDI indices for April 11, 1999 VGT image.....	42
Figure 6.8	Snow cover estimations with the F and SNDI indices for the April 2, 1999 VGT image.....	44
Figure 6.9	Snow cover estimation for various land use classes using integration of HRV pixels on areas corresponding to VGT pixels. (April 2, 1999).....	45
Figure 6.10	Snow cover distribution at the sub-pixel level on April 2, 1999.....	49
Figure 6.11	Snow cover distribution at the sub-pixel level on April 11, 1999.....	51
Figure 6.12	Snow cover distribution at the sub-pixel level in Southern Quebec on the 2 <sup>nd</sup> of April, 1999. ...	52
Figure 6.13	Snow cover distribution at the sub-pixel level in Southern Quebec on the 11 <sup>th</sup> of April, 1999. ...	53

# 1 INTRODUCTION

---

In the final report for the Pre-Launch Phase of the project, we have presented the methodology that we wanted to use to process the actual VEGETATION data, together with an application of this methodology to simulated VEGETATION and HRVIR images from TM data (Fortin et al., 1998).

In this report, we will present first a relatively short review of that report, in order to remind the methodology and the main results of the pre-launch phase. This will be followed by information concerning data acquisition related to both VEGETATION and HRVIR data during the post-launch phase. The various steps of the processing methodology of the actual data will be explained next. A discussion of the results and a conclusion will complete the report.



## 2 OBJECTIVES OF THE INVESTIGATION

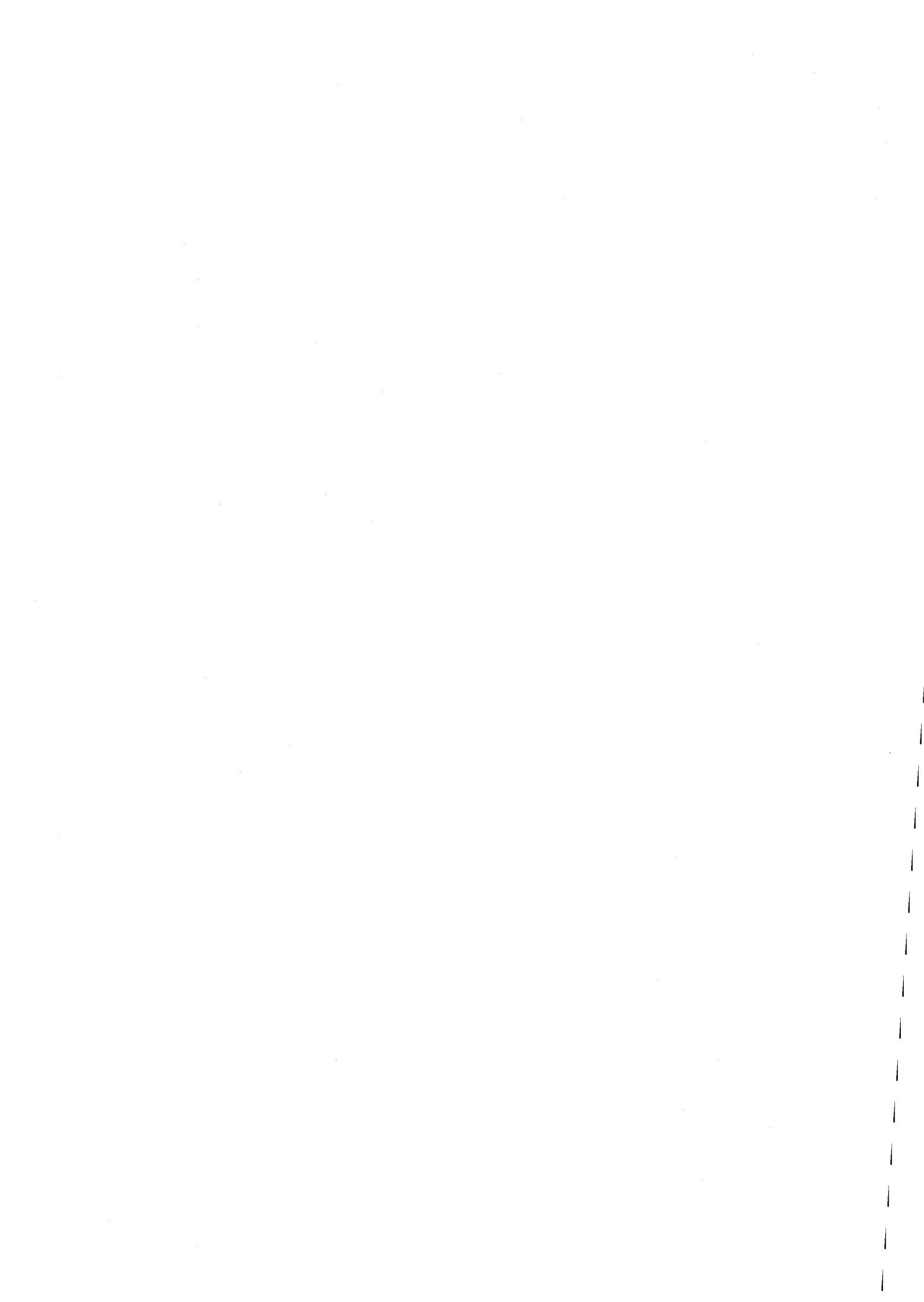
---

The general objectives of the investigation are:

- Estimation of surface variables using data from a medium spatial resolution and high frequency remote sensing sensor in orbit.
- Increased accuracy of spatial registration for multitemporal analysis of data.

Derived from those are the following specific objectives:

- Estimation of physical variables of the surface, corresponding to each land cover within the pixel, the albedo for example.
- Estimation at the sub-pixel level of the spatial distribution of snow cover on the ground.
- As accurate as possible registration of the images for multitemporal input into a spatially distributed hydrological model using geocoded data.



### **3 APPROACH USED DURING THE PRE-LAUNCH PHASE OF INVESTIGATION**

---

During the pre-launch phase of investigation, the approach has consisted (Fortin et al., 1998) in simulating first VGT and HRVIR data from TM data, the differences in bandwidths being acceptable for our purposes. The other activities were on the development and testing of our methodology based on the application of the spectral mixture theory, in order to meet the objectives of the investigation. Development and testing have been undertaken on small simulated VGT images obtained from TM data.

#### **3.1 Simulation of SPOT-4 HRVIR and VGT images**

##### **3.1.1 Introduction**

Since we estimated that five of the TM bands could be considered as sufficiently good approximations of the selected spectral bands that we will find for both SPOT-4 sensors and that it was already a satellite borne sensor, we believed that it was a good basis for simulation of the future sensors. The TM2, TM3, TM4 and TM5 bands have been used to simulate the corresponding HRVIR bands, whereas the TM1, TM3, TM4 and TM5 bands were used for VGT. Another advantage of using a satellite borne sensor like TM was simulation of simultaneous data acquisition from the future HRVIR and VGT sensors under the same orbital and atmospheric conditions.

The experimental sites are located in Southern Québec, on the South shore of the St. Lawrence river, and are representatives of the conditions encountered in that region (Fig. 3.1). Various land types can be found, including water surfaces, agricultural fields, waste and wet lands, forested areas (both conifers and deciduous) and urban areas. One of the image (Nicolet region, 9 May 1993) is taken in spring over a relatively flat area. Another one (La Chaudière watershed, 28 August 1995) is a summer image over a more hilly area, while the third one (St.François watershed, 2 April 1988), a little to the South-West of the second one, is an early spring image with partial snow cover over the same type of terrain.

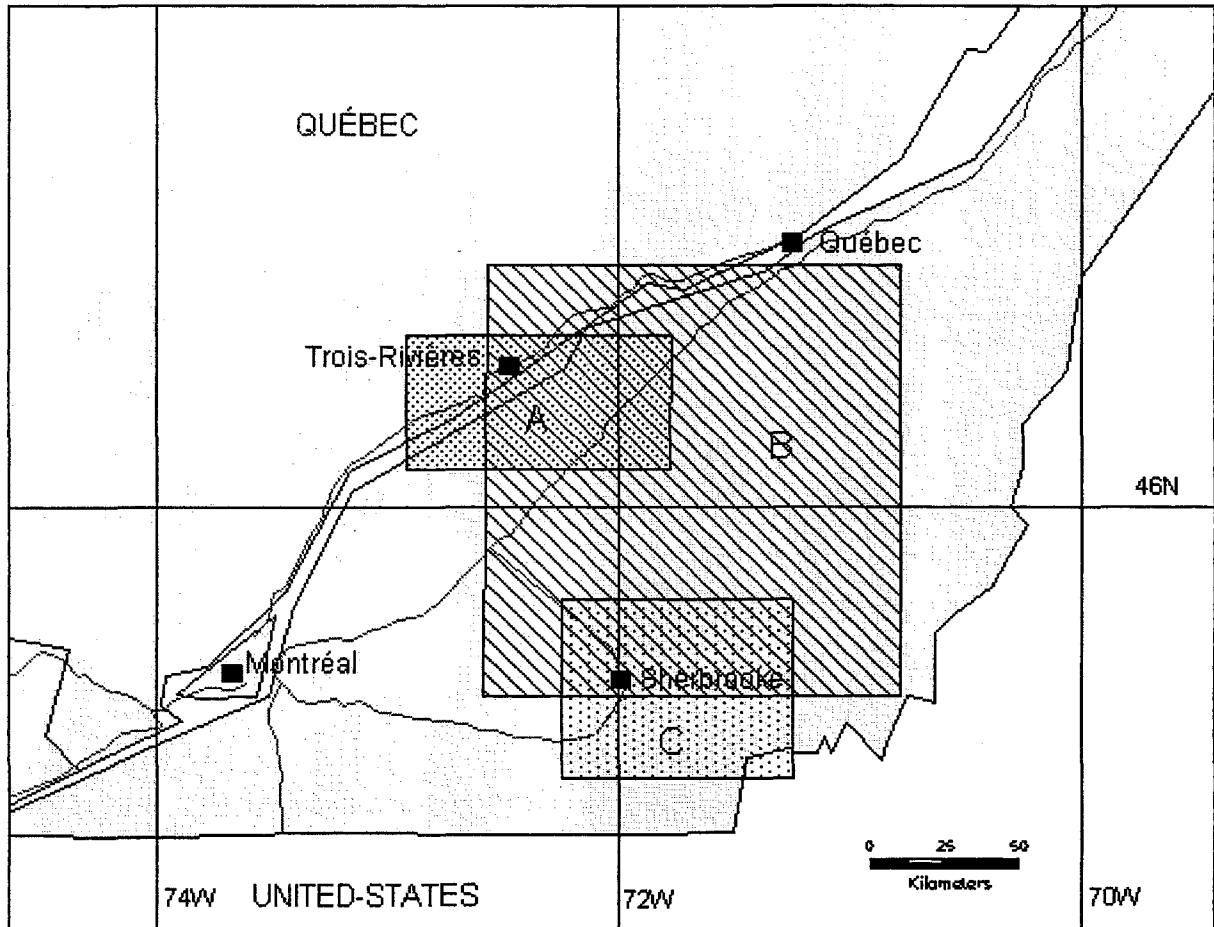


Figure 3.1 Areas covered by each of the three images used in the project  
(A) Nicolet - Trois-Rivières region  
(B) Southern Quebec, between the St-François and the Chaudière rivers;  
(C) St-François watershed

### 3.1.2 Simulation of HRVIR and VGT data

After correcting the TM images for atmospheric effects, the next step was the simulation the HRVIR 20-m resolution images. This was made using a nearest neighbor resampling procedure to change the original 25-m geocoded TM data to simulated 20-m HRVIR data. Since both resolutions are approximately the same, it had the advantage of retaining the original digital counts. The simulated 20-m HRVIR data was subsequently used to prepare a land-use classification of the area.

As for the simulation of the VEGETATION images, a simple 46 x 46 mean filter has finally been applied to the TM data already corrected for atmospheric effects in order to simulate the VGT pixels.

## 3.2 Processing of simulated VGT data for estimation of the mean reflectances of land use classes in a specific geographical area

### 3.2.1 Chosen approach assuming perfect registration of the images

According to the spectral mixture theory, the reflectance of a pixel can be considered as the linear weighted mean of the reflectances of the surface elements in the pixel. In our case, the relation between the reflectance of a VGT pixel and that of corresponding HRVIR pixels can be written, for each spectral band as:

$$R_i = \sum_{j=1}^n f_{ij} r_j + \epsilon_i \quad 0 \leq r_j \leq 1 \quad (3.1)$$

where :  $R_i$  is the reflectance of the VGT pixel  $i$ ,  $f_{ij}$  is the fraction of pixel  $i$  occupied by land use class  $j$ ,  $r_j$  is the mean reflectance of land use class  $j$  in the considered spectral band,  $\epsilon_i$  is an error term for the spectral band, taking into account measurement errors and variability of  $r_j$ , and  $n$  is the number of land use classes.

Knowing the reflectances of the VGT pixels and the fraction of each land use class in each VGT pixel, assuming perfect registration, we have to select the pixels and the number of groups of pixels that should furnish the best results using the least squares algorithm. Our approach consists in selecting  $K$  groups of pixels and estimating reflectances for each land use, using these groups and the spectral mixture theory. As slightly different results should be reached using data from these groups,

taking the mean of these estimations should lead to even better estimations. In any case, however, the fundamental problem lies in the selection of the pixels for each of these groups.

When only one group of pixels is chosen, the pixel selection procedure consists in choosing first the best pixels in each land use class,  $M^1_1, M^1_2, \dots, M^1_n$ , and then  $n$  other pixels chosen randomly among the pixels of the VGT image. Thus,  $2n$  pixels are used to solve the system of equations. Completing the group of  $n$  best pixels by  $n$  randomly chosen pixels leads to more stable results and to a good reflectance estimation even for less represented classes. To obtain even better results, using the chosen procedure, ten trials are done, keeping the  $n$  best pixels but reselecting the random pixels each time. The resulting relative errors are thus mean values of the ten trials.

Instead of selecting only one group of pixels, one can consider simultaneously  $K$  groups of VGT pixels and proceed to the estimation of the reflectances using each of these groups. Then, the mean of the estimated values in each of these groups will be considered as the estimated reflectance for each class and each spectral band. Taking the mean value helps to reduce the estimation errors made by anyone group. As pixels within each group should be selected so that all groups of pixels lead to equally reliable estimations, the elements of these vectors are randomly swapped, prior to the addition of randomly selected pixels, so that all best pixels are not in the same group.

In order to find out the optimal number of groups, the procedure consists in selecting various numbers of groups, from 2 to  $K$ , and then, using each one of these  $k$  ( $k=2, K$ ) groups, in proceeding to ten trials with both a new selection of the random pixels and a new permutation of the best pixels. Since the mean reflectances of each class are known it is possible to compare the estimated reflectances to these values and find out how many groups will give the best results.

### **3.2.2 Estimation of the co-location accuracy in an operational context**

In an operational context, the registration errors will be unknown but should be within the expected values. Also, normally it will not be possible to compare the reflectances estimated from mixed VGT pixels to those of pure HRVIR pixels taken at the same time. One exception will be the area covered by both VGT and HRVIR images, when both images are taken at the same time, but even in that case there is the possibility of a co-location error of approximately 300m.

There is still a possibility to find out a best match between the land use map and a VGT image for which the registration error is unknown. As it is not possible to modify the reflectances of the VGT image, we shift the grid superimposed on the classified HRVIR image for estimation of the

percentages of each land use class in the VGT pixels. By doing so it is possible to create percentages of land use classes for various shifts, one of these shifts being that of the VGT image. The reflectances for each land use class and each spectral band are then computed using  $k$  groups of VGT pixels. The true shift is unknown. However, it should be remembered that our method consists in taking the mean of the estimations made by each of the  $k$  groups. Then, it is possible to compute the standard deviation of these estimations. The most probable shift should be the one for which the standard deviation is the smallest. Using that criterion, it is possible to obtain a better registration accuracy.

In practice, two methods are used to perform the search for the best accuracy. The first one consists in an exhaustive procedure. The grid superimposed on the classified HRVIR image is shifted in both directions, with a distance increment of 50 m, for example, to find out the location where the lowest standard deviation for reflectance estimation is reached. It should be understood that as the fit between the position of the classified HRVIR image and the VGT image becomes more and more accurate the values of the reflectances estimated from any of the  $K$  groups of pixels should become more and more identical, such that the standard deviation between estimations becomes smaller and smaller.

The second one is an heuristic hill-climbing procedure. As in the previous procedure, both a search distance and distance increment have to be defined. Normally, this procedure is less time consuming than the first one, but one should be aware of the possibility of reaching a local minimum, thus missing the desired minimum and registration accuracy. One possibility is then to find first the area where the minimum should lie, using the exhaustive procedure with a larger distance increment and using the heuristic procedure in the vicinity of the probable minimum to get a more precise location.

In the case of VGT images, four spectral bands are available. The estimated misregistration between bands for a specific image being not more than 120m RMS, the locations estimated for each of the four spectral bands should be relatively close to each other. If this is not so, the possibility of at least one location being that of a local minimum is there. This could be a good way to verify the first results and make any necessary correction.

### 3.3 Processing of simulated VGT data for the estimation of the percentages of snow cover present in each broad land use class of any VGT pixel in a specific geographical area

#### 3.3.1 The spectral mixture approach in the case of a VGT image with partial snow cover

In the general case where the needed variable is the percentage  $p_{ij}$  of occupation of each land use class in each pixel rather than the mean reflectance of those classes, equation 3.1 is still applicable. However, in that case the number of possible land use classes, or endmembers, is limited by the number of uncorrelated spectral bands available, that is more uncorrelated bands than endmembers are required (Kerdiles and Grondona, 1995; Shimabukuro et al., 1997; Novo and Shimabukuro, 1997). Kerdiles and Grondona (1995) explain that it is possible to incorporate various dates to obtain more bands than endmembers. However, they mention that the percentages  $p_{ij}$  must be constant over the selected dates and that the endmembers reflectances must be known.

Let us consider a VGT image with a partial snow cover. Because of the dimensions of a VGT pixel, a large number of land use classes can be present at the same time. Then, in the case where the percentages of snow covered areas are needed for each of the selected land use classes, the spectral mixture equation can be written:

$$R_i = R_{i_f} + \sum_{j=1}^N p_{ij_s} (r_{j_s} - r_{j_f}) + \varepsilon_i \quad (3.2)$$

where :

$$R_{i_f} = \sum_{j=1}^N p_{ij_f} r_{j_f} \quad (3.3)$$

and:

- $R_i$  = reflectance of VGT pixel i with a possible snow cover from 0 to 100%;
- $R_{i_f}$  = reflectance of VGT pixel i under snowfree fall conditions;
- $r_{j_s}$  = reflectance of land use class j under snow cover conditions;
- $r_{j_f}$  = reflectance of land use class j under snowfree fall conditions;
- $p_{ij_s}$  = percentage of pixel i occupied by land use class j, with snow cover conditions;

- $p_{ijf}$  = percentage of pixel  $i$  occupied by land use class  $j$ , under snowfree conditions;  
 $\epsilon_i$  = error term for the spectral band taking into account measurement errors and variability of  $r$ ;  
 $N$  = number of land use classes.

It does seem unlikely that Kerdiles and Grondona (1995) suggestion can be respected, as more than one VGT image would be necessary and both reflectances of land use classes and the percentages of snow covered area over each of the total area occupied by each land use class change rapidly during the snowmelt period.

Another solution can, however, be put forward as a single spring image could be used to find out the total percentage of snow cover on each pixel with a relatively good accuracy. Once that percentage is done, it could be possible to distribute that percentage among the various land use classes, knowing that snow will disappear first in open areas, then in deciduous forested areas and finally in coniferous forests. As the resulting partial snow cover map will, at least in a few applications, be used to update the snow cover in a hydrological model for snowmelt forecasting, the informations furnished by that model could, in turn, help to distribute the total snow covered area on each pixel among the land use classes present on that pixel.

Two indices are suggested to find out the total snow covered area on each pixel. Both are based on the effect of the snow reflectance on the ground cover as compared to snowfree reflectances of the various land uses. Let us first remember that equation 3.3 gives the relation between the endmember reflectances and the VGT pixel reflectance for snowfree conditions, either in fall or in spring. A similar equation can be written for complete snow cover conditions for the same land use classes.

$$R_{i_s} = \sum_{j=1}^N p_{ij_s} r_{j_s} \quad (3.4)$$

Where:

- $R_{i_s}$  = reflectance of VGT pixel  $i$  under snow cover conditions;  
 $r_{j_s}$  = reflectance of land use class  $j$  under snow cover conditions;  
 $p_{ij_s}$  = percentage of pixel  $i$  occupied by land use class  $j$ , with snow cover conditions;  
 $N$  = number of land use classes.

Finally, the reflectance of pixel  $i$  under partial snow cover conditions is given by equation 3.2. It is then possible to suggest a first relation:

$$F = \frac{R_i - R_{i_f}}{R_{i_s} - R_{i_f}} \quad (3.5)$$

It can be seen rapidly that, for a given pixel,  $F$  will go from a value of 1, when the snow cover is complete and the reflectances of the land use classes are identical to those used at the denominator, to a value of 0, under snowfree conditions identical to those used for the fall or spring reference image. The value of  $F$  between those two extremes will be a function of the amount of snow cover on each of the land use classes present on the pixel, as it can be understood from equation 3.2.

A relation similar to the NDVI, which we will call the normalized difference snow index, NDSI, can also be derived:

$$NDSI = \frac{R_i - R_{i_f}}{R_i + R_{i_f}} \quad (3.6)$$

### 3.3.2 Description of the chosen approach

In the case of partial snow cover when the needed variable is the fraction of snow cover on each individual pixel for each of the land use classes present on the pixel, the chosen approach is similar to that explained before. Once the position of the VGT image is known as accurately as possible, we can proceed to the estimation of percentages of snow cover for each of the land use classes on a pixel by pixel basis.

## **4 MAIN RESULTS OBTAINED DURING THE PRE-LAUNCH PHASE OF THE INVESTIGATION**

---

The first chapters of this report have permitted to review the main points regarding the methodology used in this investigation. In this chapter, the results obtained during that phase will also be reviewed in preparation for the discussion of the results obtained with the actual VGT images.

### **4.1 Determination of the actual position of a VGT image relative to its expected position**

Let us recall here that in an operational context, the exact position of a specific VGT image is not known, but that it is possible to recompute the percentage of occupation of each land use class on each VGT pixel, assuming various shifts. Computation of the relative error between the estimated reflectances from VGT pixels and the true values, as estimated from corresponding HRVIR pixels, for each VGT band, as a function of the number of pixel groups, has led to the conclusion that four (4) groups of pixels would give the best results.

As four groups of pixels are used, the position for which the estimated reflectances by each of these four groups are the more similar should be the sought position. In practice, we should look for the lowest standard deviation estimated from the values furnished by each of the groups.

The estimation of the expected position of a VGT image, as well as the estimation of the reflectances of the land use classes present on the image, were done based on the TM image taken on the 28th of August 1995. Using the exhaustive method implying detailed standard deviation mapping, a maximum shift of 300m has been assumed in each direction, defining a search area of 600 x 600m centered on the expected true location. A grid size of 50m has been selected to perform the computations, resulting in 169 values from which a map could be drawn.

This exhaustive computation was performed for each of 6 simulated VGT images, with various shifts relative to the expected «true» location (0,0). The shifted locations, in meters, were: (0,0), (-250,100), (250,-150), (-50,-275), (200,200) for the first five images, assuming perfect multispectral registration. For the sixth image, each band had a different location (200,-200) for B2, (175,-225) for B3 and (225,-150) for B4.

It was found out that most maps did have relatively smooth gradients, allowing a slow degradation of the results as the distance between the estimated position and the «true» position increased. This meant that a perfect fit between the VGT image and the classified HRVIR image was not a must as long as the standard deviation did not increase too much. For each of the six cases, the exact location was estimated within 100m and as near as 10m in one case. The heuristic search gave results between 27 and 153 meters, a few of them being closer to the true location than the exhaustive search. Those distances were considered as acceptable as both the estimated and the «true» locations were in areas of relatively low standard deviation gradients.

## **4.2 Determination of the reflectances of the land use classes**

Knowing that it was possible to locate the VGT images with a very good accuracy, we have verified if the mean reflectances of the various land use classes could also be estimated with a good accuracy. The results are presented in table 4.1 and figure 4.1. It can be seen that both search methods allow a very good estimation of the mean reflectances for each of the spectral bands. The estimated reflectances for “urban areas and roads” is less accurate, but it is still within one standard deviation from the mean value estimated from HRVIR pixels.

Table 4.1 Estimated land use reflectances from the VGT spectral bands vs HRVIR reflectances, at location (0,0) for the August 28<sup>th</sup> 1995 simulated images.

## B-2 Band

Land use classes	Identification	HRVIR Reflectances		Estim. reflectances from VGT	
		% of occupations	Mean %	Standard deviation %	Standard error
Urban areas and roads	4.6	7.4	3.1	10.3	10.29
Pastures and alfalfa	14.6	4.6	0.9	4.4	4.32
Cereals	8.8	5.5	0.9	5.4	5.4
Corn	3.9	4.8	0.4	5.2	5
Water	3.9	2.7	0.7	2.1	2.02
Wet lands	6.0	5.4	1.0	4.5	4.48
Bare soils	8.6	9.6	3.2	9.7	9.68
Herbacious fallow lands and bushes	15.9	3.3	0.9	2.8	2.74
Mixed forest	23.5	2.4	0.4	2.0	2
Coniferous forests	10.4	2.3	0.4	1.8	1.79

## B-3 Band

Land use classes	HRVIR Reflectances		Estim. reflectances from VGT	
	Mean %	Standard deviation %	Standard error	Heuristic
Urban areas and roads	27.2	6.5	21.2	20.86
Pastures and alfalfa	45.0	5.8	49.2	49.24
Cereals	36.9	2.5	35.7	35.38
Corn	42.1	2.4	43.5	42.69
Water	2.7	3.4	1.2	1.56
Wet lands	28.7	3.7	27.7	28.01
Bare soils	31.2	5.0	29.5	29.89
Herbacious fallow lands and bushes	32.7	3.1	32.5	31.94
Mixed forest	34.6	4.1	35.6	35.8
Coniferous forests	24.6	2.8	21.6	21.68

## B-4 Band

Land use classes	HRVIR Reflectances		Estimated reflectances from VGT	
	Mean %	Standard deviation %	Standard error mapping	Heuristic Research
Urban areas and roads	18.3	4.3	17.5	17.25
Pastures and alfalfa	21.9	2.0	22.16	22.21
Cereals	24.8	1.9	25.73	25.79
Corn	19.2	1.0	19.18	18.79
Water	0.7	1.5	0.07	0.06
Wet lands	18.2	2.1	17.4	17.44
Bare soils	27.1	3.4	27.9	28.05
Herbacious fallow lands and bushes	17.5	2.2	17.5	17.3
Mixed forest	14.9	2.0	14.88	15.04
Coniferous forests	10.4	1.5	9.09	8.93

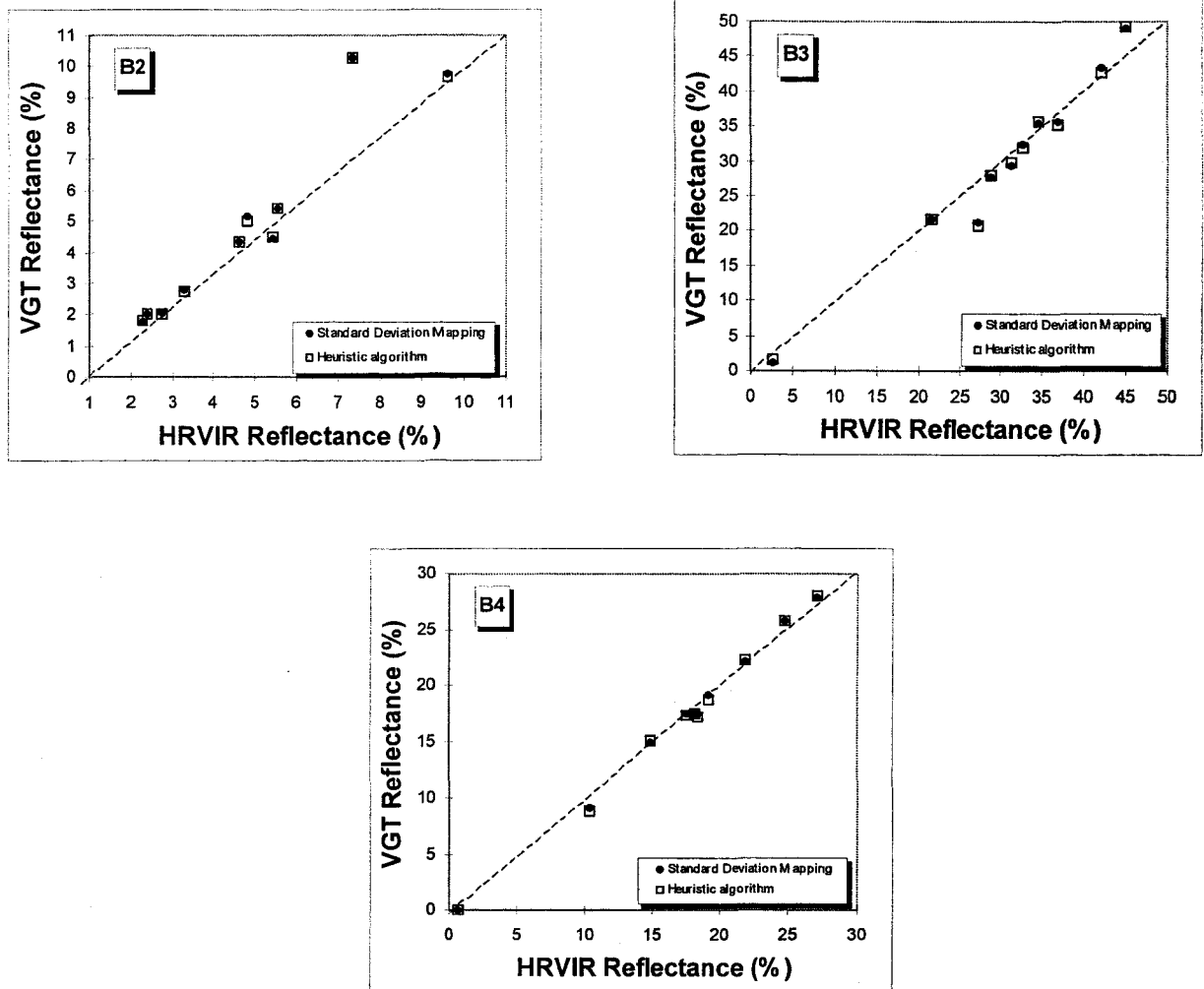


Figure 4.1 VGT estimated reflectances VS HRVIR reflectances

### **4.3 Determination of the snow cover percentages at the sub-pixel level**

#### **4.3.1 Main characteristics of the HRVIR and VGT images**

The original TM images for partial snow cover over Southern Québec (figure 3.1) was taken on the 3rd of April 1988 at 9:30 local time. It corresponds to a quarter of a full TM image. As it was shown that it was possible to locate the VGT images normally with an accuracy better than 100m, the emphasis was put essentially on the information that could be obtained from VGT images. A perfect fit was assumed as the standard deviation did not increase too much within that distance from the true location of the image.

Seven classes were selected on the image (table 4.2). Water surfaces occupy 2.6% of the area, of which 0.7% are frozen, whereas open areas occupy 43.5%, of which 19.1% are covered with snow. Deciduous forests occupy 26.8%, of which 21.1% are covered with snow, and, finally, coniferous forests occupy 27.1% of the image and are completely covered with snow. It was impossible to distinguish between snow covered and snowfree coniferous forests, but a careful examination of the image showed us that coniferous forests were mostly surrounded by other land use classes on which there still was snow.

#### **4.3.2 Sub-pixel estimation of snow cover**

The difficulties that would likely be encountered for the estimation of snow cover on each individual land use class present on a single VGT pixel have been discussed in section 3.3. In particular, it was mentioned that the estimation of those percentages would be possible only if the reflectances were known and the number of endmembers, that is of land use classes, would be in agreement with the number of independent bands. In practice, those conditions were not satisfied with the image that we had and no worthwhile results could be obtained. There were more land use classes than bands.

Table 4.2 Mean reflectances (standard deviation) and percentage of occupation of each identified land use classes on the spring image (April 2, 1988).

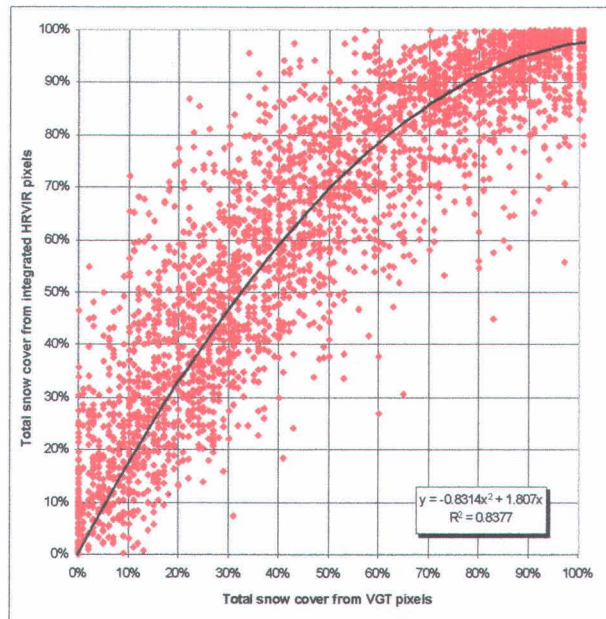
Land use classes	% of land use occupation	Reflectance (%)							
		HRVIR1		HRVIR2		HRVIR3		HRVIR4	
		Mean (%)	SD (%)	Mean (%)	SD (%)	Mean (%)	SD (%)	Mean (%)	SD (%)
Coniferous forest (with snow)	27.1	10.8	5.3	10.5	4.9	26.5	4.6	8.8	1.5
Coniferous forest (without snow)	0.0								
Deciduous forest (with snow)	21.1	26.1	7.2	28.0	7.1	35.7	5.6	9.7	1.6
Deciduous forest (without snow)	5.7	9.4	3.0	10.6	2.9	26.9	3.7	19.1	5.0
Open areas (with snow)	19.1	32.5	13.2	34.6	13.1	44.4	10.2	11.3	5.1
Open areas (without snow)	24.4	13.8	4.4	17.0	4.6	29.7	7.4	28.9	9.0
Lakes and rivers (frozen)	0.7	50.4	11.5	47.8	11.0	33.2	10.0	1.9	0.8
Lakes and rivers (unfrozen)	1.9	12.7	8.3	12.7	7.8	12.9	6.8	5.5	3.8

We, then, have concentrated our attention on finding the total percentage of snow cover on each pixel using either equation 3.5 or 3.6. Let us look at the results from equation 3.5. Equation 3.5 is based on the assumption that the reflectance of a partially snow covered pixel will lie somewhere between that corresponding to snowfree conditions and that corresponding to snow covered conditions. In normal operations, single VGT images or mosaics corresponding to those conditions would be available. In our case, no such images were of course available. So, we have created both a complete snow cover image and a snowfree image using the mean class reflectances of table 4.2 and the mixing theory. It should be clear that these images represent only an approximation of the images that should be used to apply equation 3.5.

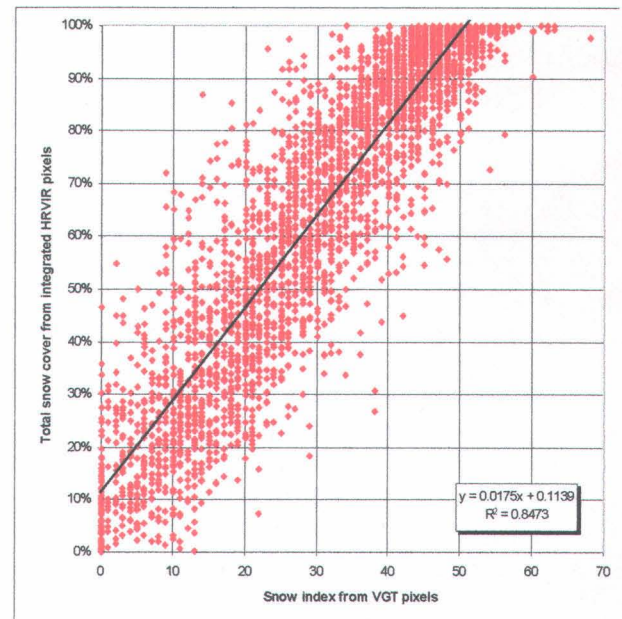
In figure 4.3a, the total percentage of snow cover on each pixel as obtained from equation 3.5, that is the value of  $F$ , is compared to the total percentage of snow cover on the same pixel, as obtained from the HRVIR pixels corresponding to that VGT pixel. It can be seen that equation 3.5 underestimates the “true” percentage of snow cover on each pixel, but that a relation could be obtained with a coefficient of determination of 0.8377. Other relations could be obtained by not forcing the relation to go through (0,0) and/or using higher degree polynomials. It should be mentioned that 3672 points are on that figure.

The relation between the normalized difference snow index (NDSI) obtained from equation 3.6 and the total percentage of snow cover on the same pixel, as estimated from the HRVIR pixels corresponding to that VGT pixel, is presented in figure 4.3b. It can be seen that it is linear and has a coefficient of determination of 0.8473, which is very close to that of the previous relation. As a temporary conclusion, it can be said that both relations will likely furnish total snow cover on each pixel with approximately the same accuracy.

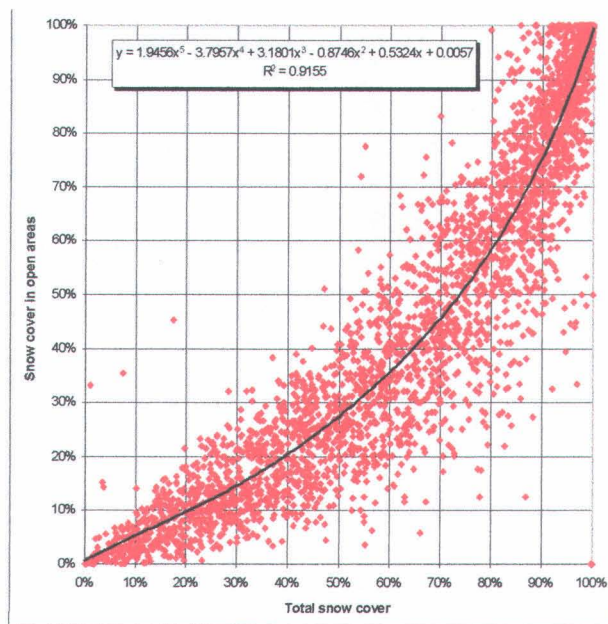
It is however possible to try to distribute that total snow cover on each pixel among each of the mean land use classes, namely coniferous forests, deciduous forest and open areas. It is clear from observations and simulation of the melt process that snow disappears first in open areas, then in deciduous forests and finally in coniferous forests. It is thus likely that, for a given percentage of snow cover on a pixel, the remaining percentage of snow in forested areas will be greater than that in open areas. This is effectively shown in figures 4.3c and 4.3d.



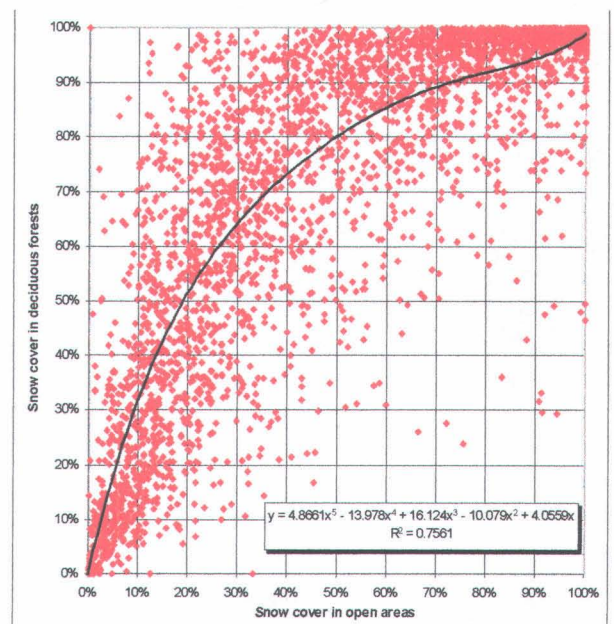
a) Total percentage of snow cover estimated from integrated HRVIR pixels as a function of the total snow cover estimated from VGT pixels (equation 3.5).



b) Total percentage of snow cover estimated from integrated HRVIR pixels as a function of the normalized difference snow index (NDSI) of equation 3.6.



c) Percentage of open areas covered by snow on each area corresponding to a VGT pixel as a function of the total area covered by snow on that pixel. Both values are from integration of HRVIR pixels.



d) Percentage of deciduous forests covered by snow on each area corresponding to a VGT pixel as a function. Open areas covered by snow on that pixel. Both values are from integration of HRVIR pixels.

Figure 4.2 Snow cover estimations on VGT pixels.

In figure 4.3c, the percentage of snow cover in open areas on a specific VGT pixel is shown as a function of the total percentage of snow cover on that same pixel. Those percentages have been obtained by summing up the snow covered and snowfree HRVIR pixels corresponding to each VGT pixel. If all VGT pixels would correspond to only one class, namely open areas more or less at the same elevation, then all points would lie on the  $y = x$  line. Since, in our case, a large number of VGT pixels are likely to include the three main land use classes, for each of these pixels, the percentage of snow covered HRVIR pixels corresponding to the open areas class will be lower than that corresponding to the total percentage of snow covered HRVIR pixels corresponding to a VGT pixel. This is what is shown in figure 4.3c. As an example, if the total snow cover on a pixel is 40%, then the snow cover in open areas is down to 20%.

Let us look now at the relation between the snow cover in deciduous forests as compared to that in open areas, which is shown in figure 4.3d. It should be remembered here that it was impossible to find out snowfree coniferous forests. One can notice readily that as the percentage of snow cover in open areas diminishes from 100% to, let us say, 50%, the percentage of snow cover in deciduous forested areas remains practically between 100% and 90% and, then, drops to zero as the percentage of snow cover continues to diminish in open areas. This behaviour confirms our assumptions. A fifth degree polynomial has been fit to the data as an example of a possible relation, but a number of other relations could be possible. For instance, we could have the percentage of snow cover in deciduous forested areas stay at 100% as long as the percentage of snow cover in open areas is greater than 50%, followed by a linear decrease to 0% from then on. It should be mentioned, finally, that a number of percentages of snow cover in deciduous forested areas are lower than the corresponding percentages in open areas. That should not be the case. The most probable reason for that is that pixels were improperly classified either in one class or the other. Fallow lands and bushes would probably be in that case.

It is finally interesting to present the information contained in figure 4.3a on a map rather than on a graph. Figure 4.4a represents the total percentage of snow cover on each VGT pixel, from 0 to 100%, as estimated from HRVIR pixels corresponding to each VGT pixel. The total snow cover estimated by equation 3.5 is presented in figure 4.4b. It was mentioned previously that equation 3.5 was underestimating the percentage of snow cover on each VGT pixel and that is noticeable in figure 4.4b, as the grey shades are darker than in figure 4.4a. One can also mention that underestimation tends to occur mostly where the percentage of snow is relatively low. If the relation between total snow cover from equation 3.5 and total snow cover from HRVIR pixels, as determined in figure 4.3a, is applied, then the resulting map is shown in figure 4.4c. It can be seen

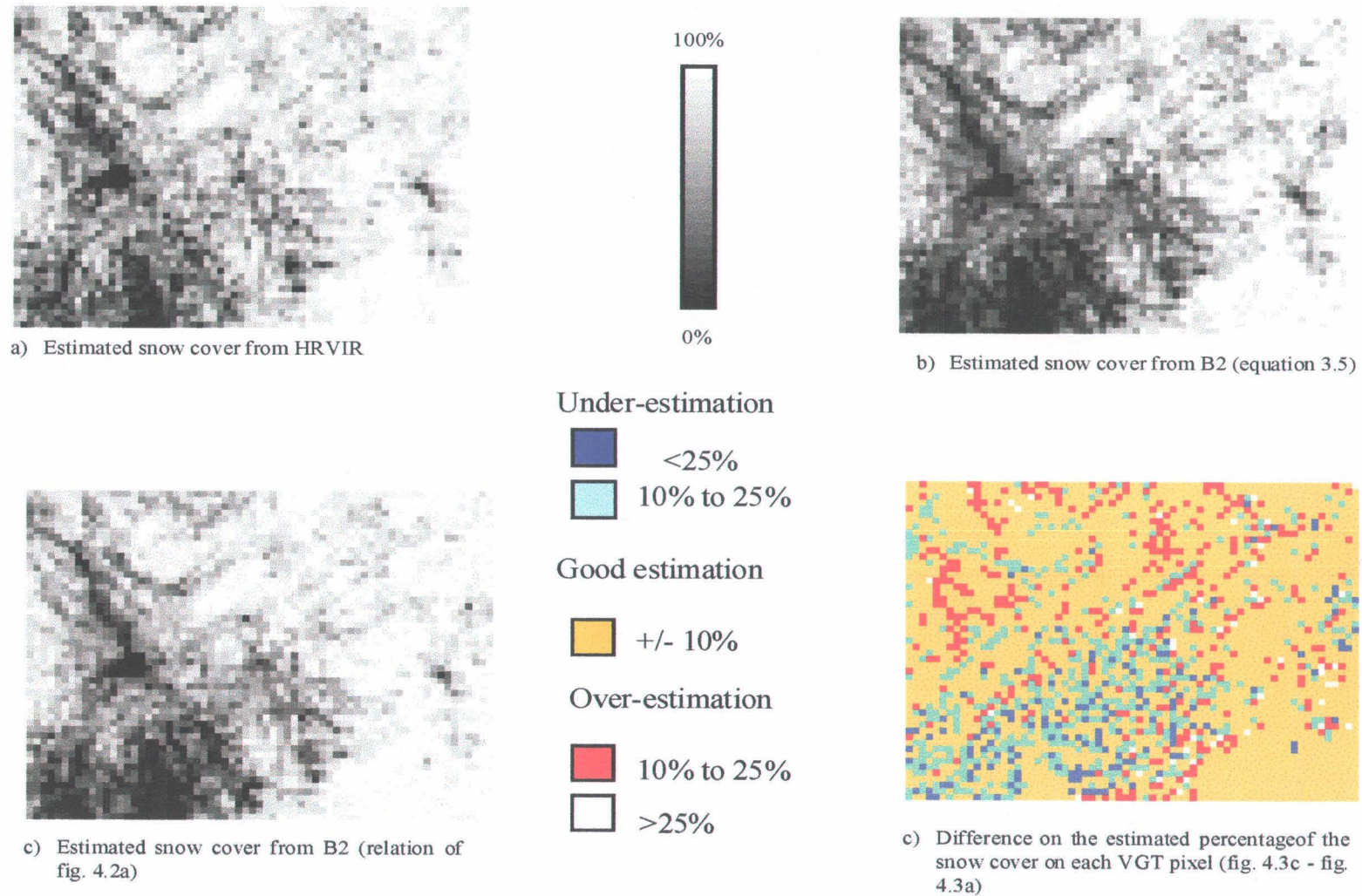


Figure 4.3 Snow cover estimation – April 2, 1988t

that this latter map is much more similar to that of figure 4.4a. The absolute estimation error of the snow cover mapping in figure 4.4c in relation to the value of figure 4.4a is shown in figure 4.4d. It can be seen that most of the snow cover estimations are within 10% of the HRVIR estimated values. More precisely, we have:

- Underestimation greater than 25% for 4.1% of the pixels;
- Underestimation between -25% and -10% for 10.3% of the pixels;
- Estimation within -10% and +10% for 70.1% of the pixels;
- Overestimation between +10% and +25% for 10.3% of the pixels;
- Overestimation greater than 25% for 1.4% of the pixels.

The results obtained on snow cover estimation show that it is possible to estimate the total percentage of snow cover on each VGT pixel with a quite satisfactory accuracy. It was also shown that it could be possible to go one step further in distributing that total snow cover among the main land use classes present on any VGT pixel. That possibility to estimate the spatial distribution of snow cover at the sub-pixel level will be very useful for hydrological simulations.



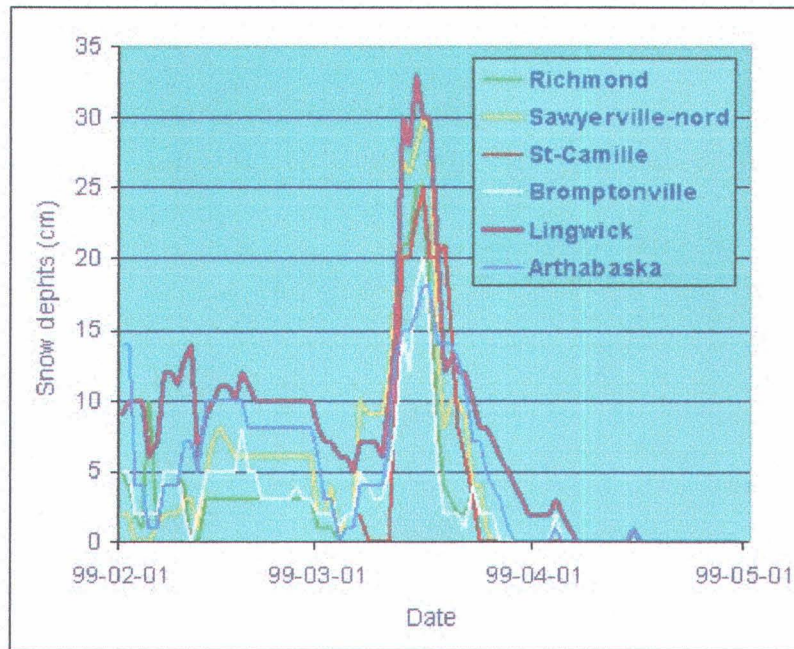
## **5 ACQUISITION OF VGT AND HRVIR IMAGES DURING THE POST-LAUNCH PHASE OF THE INVESTIGATION**

---

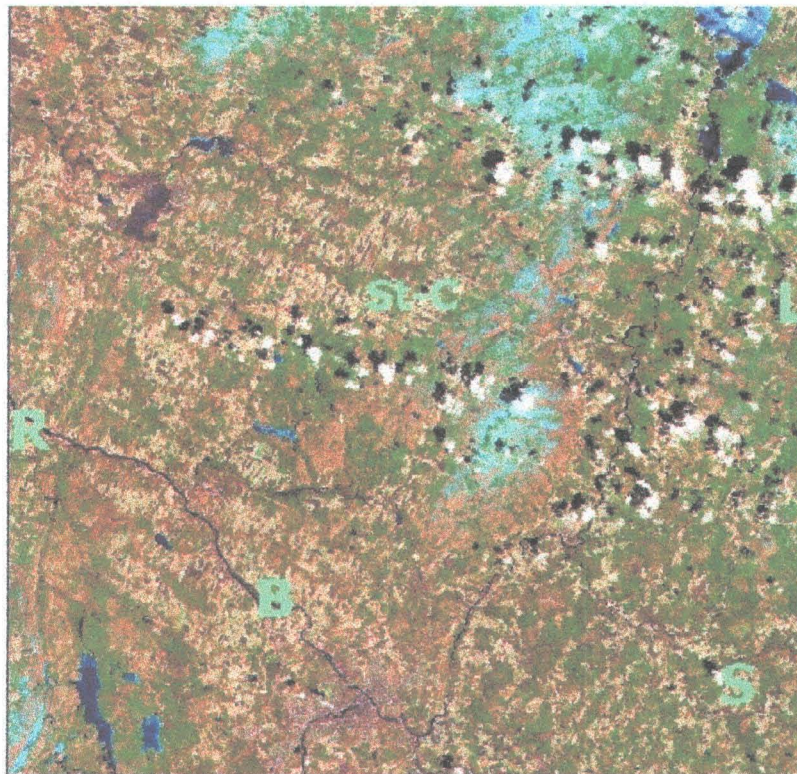
### **5.1 Spatio-temporal evolution of the snow cover in Southern Québec during the 1998-1999 winter**

Ideally, we would have like to have a winter scene with full snow cover and reflectance values close to those that are encountered just before snowmelt begins. The partial snow cover image (area corresponding to a HRVIR image taken simultaneously to the VGT image) needed to test our methodology had to have a snow cover distribution similar to that which we had for simulation, in order to be able to find out valuable answers for all land use classes. As for the snowfree image, it had to be taken after complete snowmelt in the region and before there was a significant change in the reflectances of the various land use classes, particularly vegetation.

Snow cover remained relatively shallow in Southern Québec during the 1998-1999 winter, particularly in the region where we wanted to compare the results obtained with actual VGT data to those previously obtained with simulated VGT data. As shown in figure 5.1, the snow cover at climatological stations in open areas, remained under approximately 5 to 10cm for January and February 1999 for most of the area covered by the HRVIR image taken on the 11th of April 1999, which is the high resolution reference image. The month of March began with that shallow snow cover, but snowfalls in the second half of the month increased snow depths to more than 20cm over the area. However, rapid snowmelt followed that increase, so that by the end of the month, the snow depths in open areas were back to less than 5cm. In April, most of the area remained snowfree. Snow cover could be found only at higher elevations to the N-E of the region.



a) Snow depths a function of time (data from Environment Quebec)



b) Locations of the climatological stations; R = Richmond, S = Sawyerville-nord, St-C = St-Camille, B = Bromptonville, L = Lingwick.

Figure 5.1 Snow cover in Southern Quebec from February to May 1999.

## 5.2 VGT and HRVIR images pre-selected for the investigation

We wanted to obtain VGT images covering the whole of Québec from South to North. So, we browsed the VEGETATION catalogue from the beginning of January to the end of June, for the area included between latitudes  $44^{\circ}$  and  $55^{\circ}$  N and longitudes  $65^{\circ}$  to  $80^{\circ}$  W. Our primary objective was the area in southern Québec corresponding to that for which the simulation images had been processed. It was also the area for which we could have more snow cover data. We also wanted, as a secondary objective, to obtain images covering the more northerly regions of Québec, namely the James Bay watersheds on which Hydro-Québec operates power plants.

In the southern regions of Québec, VGT images were available in February, but very few in March, due to increased cloud cover. Five VGT images were pre-selected during those months as possible full snow cover reference images with relatively cloud-free conditions for a sufficiently large area (table 5.1).

The choice of the VGT images for partial snow cover over southern Québec was essentially controlled by the availability of high resolution HRVIR data. The only HRVIR image available over the area for conditions of partial snow cover was taken on the 11th of April (table 5.1), following our request to Spot-Image for image acquisition. Most of the snow cover has melted and there are lines of small cumulus clouds in the middle of the image. Both these clouds and their shadows affect the identification of snow cover as they are unfortunately where they should not be. A panchromatic image taken by SPOT-2 was also available on the 2nd of April. The identification of snow cover in the panchromatic image is somewhat limited by the fact that only one band is available, but there is still a sufficiently large fraction of the image covered with snow. Put in other words, both images do not constitute very good high resolution reference images for our purposes. So, in April, we have pre-selected three VGT images for days including those on which the high resolution images were available.

Five more VGT images were pre-selected in May and one more in June. Those taken at the beginning of May were considered as potential snowfree reference images. At the same time, the VGT images taken with full snow cover over more northerly region of Québec could be considered as potential full cover reference images for those regions, those coming later as partial snow cover images and those taken at the end as snowfree images. Also, all those images were selected with the idea to cover the largest area possible in Québec with the minimum of images for the desired snow and snowfree conditions.

Finally, we should mention that the VGT images were only available according to an Albers conic projection, whereas we are using Lambert conic projection for large regions over Canada.

Table 5.1 Acquisition of SPOT images in 1999

Satellite	Sensor	Month	Date	Identification
SPOT-4	VEGETATION	January	20	19990129B056
			8	19990208E144
		February	23	19990223E153
			5	19990305E010
			27	19990327E032
		March	2	19990402E250
			5	19990405E106
			11	19990411E053
		April	2	19990502E219
			6	19990506E091
			11	19990511E248
			15	19990515E127
			24	19990524E157
		May	8	19990608E116
			12	19990612E246
11	19990611E248			
SPOT-4	HRVIR	April	11	4 628-258 990411 155433 1I / 0
SPOT-2	PANCHRO	April	2	2 628-258 990402 155555 2p / 0

## 6 PROCESSING OF THE ACTUAL VEGETATION AND HRVIR IMAGES

---

### 6.1 Atmospheric corrections

Proceeding to atmospheric corrections on the VGT and HRVIR data was not easy at all and a lot of time was spent to find out solutions. First, most, if not all, commercial software packages were not updated to make atmospheric corrections for the SPOT-4 data. We are using the Easy-Pace software from PCI Geomatics.

Let us begin with HRVIR data. It was possible to correct the first three bands (B1, B2 and B3) of the April 11th image with the Easy-Pace software, but that software does not allow correction of the B4 band in the infrared. So, the B4 band remained uncorrected for atmospheric effects. For the other three bands, the digital counts did not change much after atmospheric correction, suggesting that atmospheric effects were not important on that day, at least for those bands.

In the case of data acquisition on the 2nd of April 1999 by the HRV panchromatic band from the SPOT-2 satellite, again the Easy-Pace software could not do it directly. So, we have corrected the panchromatic band for atmospheric effects assuming it was not too much different from the B2 band.

The four VGT bands have been corrected using SMAC (Rahman and Dedieu, 1994). That program was difficult to obtain and was allowing correction of atmospheric effects on only one pixel was the program was run. So, we had to modify the program to allow lecture and correction of complete images.

## 6.2 Geometric corrections

### 6.2.1 HRVIR and HRV images

Geometric corrections of the high resolution HRVIR and HRV images were done using an image-to-image procedure, the reference image being a TM image previously resampled to 20-m for the simulation of the SPOT-4 images and projected according to UTM coordinates. The output HRVIR and HRV images were projected according to the Albers conical equal area projection applied on VGT images.

### 6.2.2 VEGETATION images

As far as VEGETATION are concerned, we had to use the images taken on the 2nd and 11th of April and two other images, one for full snow cover and one for snowfree conditions. The parameters of the projected images according to an Albers conical equal area projection were not identical. On the other hand, one full snow cover image (Feb. 8, 1999) and one snowfree image (May 2, 1999) had exactly the same projection parameters as that of the April 11 image so that it was possible to superimpose them. It remained to perform a geometric correction of the April 2 image using an image-to-image procedure with the April 11 image as reference image.

### 6.2.3 Relative location of the VEGETATION images between themselves and with respect to the HRVIR images

The multitemporal registration accuracy  $x_T$  expected in the pre-launch specifications was smaller than 0.5km with the objective of reaching 0.3km, whereas the multispectral registration accuracy  $x_S$  was to be clearly smaller than 0.3km, with an objective of 0.1km. The co-location between the mean spectral location and high resolution pixel resolution was to be smaller than 0.3km.

The «preliminary budget for geometrical performance» shown at the final pre-launch meeting in September 1998 indicated that those specifications and objectives would be reached for most points, using GCP corrections. It was expected at that meeting that the multitemporal accuracy  $x_T$  with GCP corrections would be 100m RMS, with a maximum value of 300m. The performances computed on VGT-P images for multispectral registration gave an  $x_S$  of 120m RMS with a maximum value of 200m RMS. As for the co-location between VGT and HRVIR images  $\delta$ , it was 255m RMS with a maximum value of 400m. It was expected that «this performance could be enhanced but not very much due to HRVIR mirror position uncertainty».

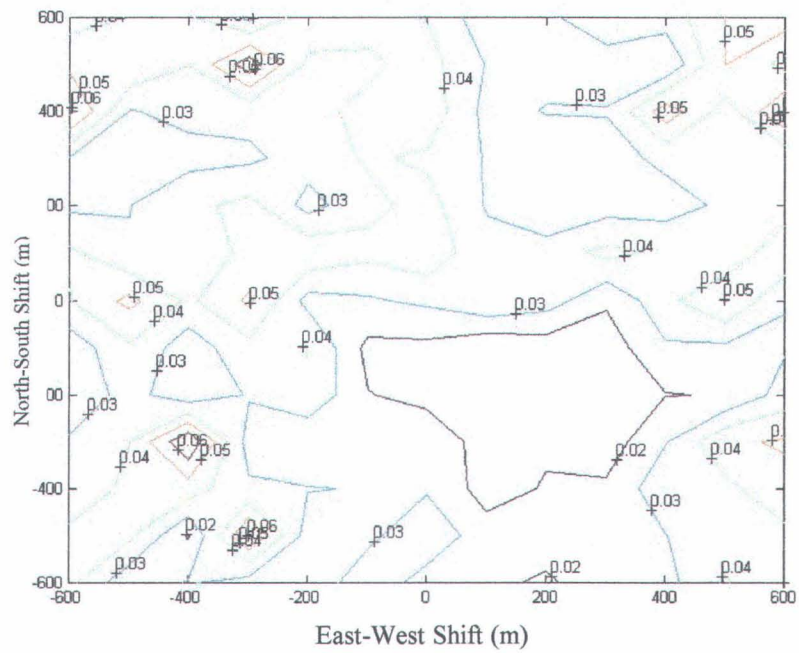
In order to obtain better results we had to find out the relative multitemporal location of the VGT images used in the investigation, as well as their co-location with the reference high resolution HRVIR image. For this purpose, we used the exhaustive search procedure explained previously in Fortin et al. (1998) and outlined in section 3.2.2. Figure 6.1a presents a standard deviation map for an area of 1200m x 1200m centered on the location of the HRVIR image. This map was obtained with computations of land use reflectances made every 100m in both directions and represents the spatial variation of the standard deviation around the mean reflectance of each land use class, in band B2, for the VGT image taken on the 2nd of May 1999. It can be found that the minimum standard deviation is in the SE quadrant. In order to find out more precisely the location of the VGT image relative to the HRVIR image, we made a zoom covering the SE quadrant of the preceding image, with computations made every 50m (figure 6.1b). Both figures indicate that there is a relatively large area in the SE quadrant in which the standard deviation is under 0.02, meaning that any location within that area should lead to approximately the same results for the estimation of the land use reflectances. Note that the minimum standard deviation value would be at (0,0) if the images could be superimposed exactly. All other maps can be found in Appendix 1.

The results obtained as far as the multitemporal and multispectral locations of the various bands of VGT images are concerned are shown in figure 6.2 and table 6.1. Let us look first at the VGT image taken simultaneously to the HRVIR image, on April 11, 1999. The B3 and B4 bands are within the RMS co-location error of 255m whereas the B2 band is within the maximum co-location error estimated at 400m. Also, the three bands do respect the specifications for the multispectral registration. The same can be observed for the other images. All of them are located in the SE quadrant and are relatively close to each other.

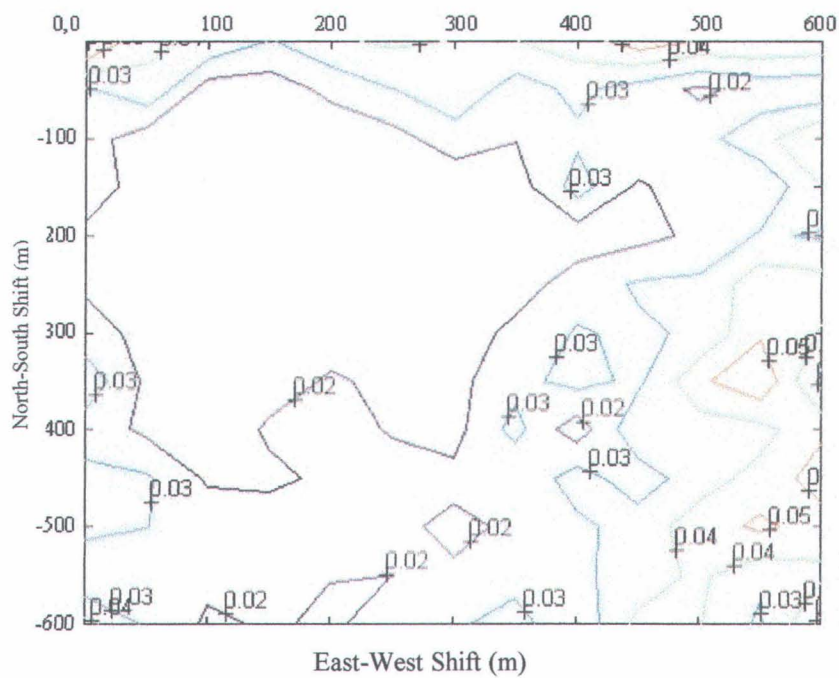
Table 6.1 Multispectral and multitemporal registration of VGT images with respect to the HRVIR image taken on April 11, 1999.

Date	Band	Relative coordinates		Distance from HRVIR (m)
		X(m)	Y(m)	
Feb 8,1999	B2	210	-350	408.2
	B3	240	-320	400
	B4	250	-350	430.1
April 2,1999*	B2	***	***	***
	B3	***	***	***
	B4	***	***	***
April 11,1999	B2	100	-350	364
	B3	0	-260	260
	B4	120	-175	212.2
May 2,1999	B2	150	-175	230.5
	B3	200	-280	344.1
	B4	300	-240	384.2

\* Only a "standard" geometric correction was performed for the April 2 VGT image (section 6.2.2).



a) 1200m X 1200m search data



b) 600m X 600m Zoom on the South-East quadrant

Figure 6.1 Standard deviation mapping for the May 2, 1999. VGT spectral band B2.

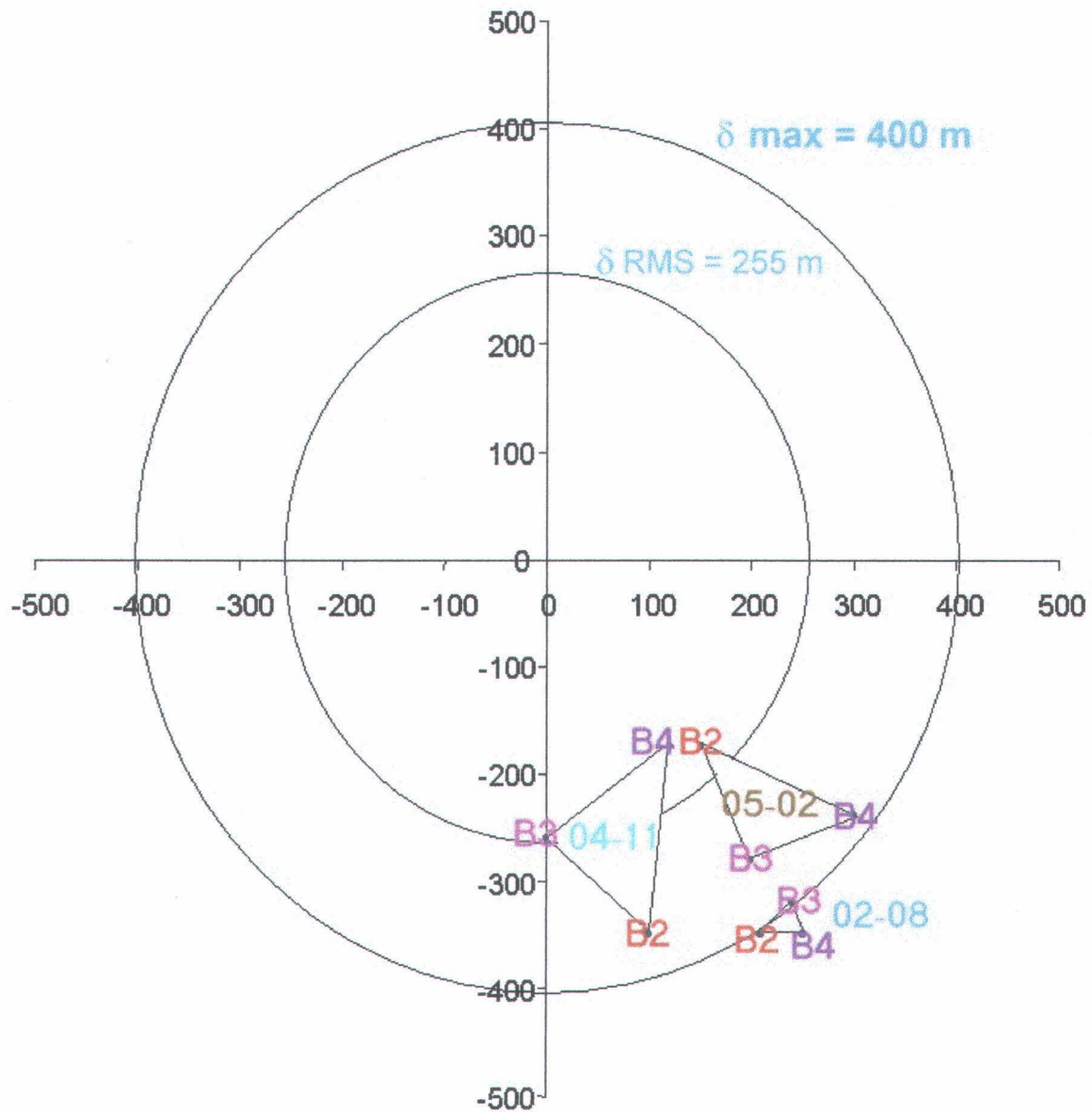


Figure 6.2 Multispectral and multitemporal registration of VGT images, with respect to the HRVIR image taken on April 11, 1999.  $\delta$  is expected co-location error between VGT and HRVIR images.

### **6.3 Estimation of land use reflectances**

Land use reflectances have been estimated for the three VGT bands for which we have similar bands on the HRVIR sensor for the images taken simultaneously on April 11, 1999. Whereas on the simulated images, land use reflectances were better estimated for the B3 and B4 bands than for the B2 band, for the actual VGT and HRVIR images better results are obtained for the B2 band than for the other two bands (figure 6.3). Still, the results can be considered as quite good, as the estimated reflectances from VGT pixels lie within one standard deviation from the mean reflectance values estimated from HRVIR pixels (table 6.2). A total of 18 classes have been kept for the estimations, leading to percentages relatively small. It is not surprising then to find out less accurate estimations. Estimations for classes corresponding to a very low percentage could not be considered as accurate and significant. So, only nine classes having higher percentages are shown in figure 6.3.

### **6.4 Estimation of snow cover at the sub-pixel level**

#### **6.4.1 Selection of VEGETATION and high resolution images (HRVIR and HRV)**

As mentioned in chapter 5, the snow cover conditions were far from being optimal in the Spring of 1999 to test the methodology previously developed using simulated data. Only one reference snowfree image is needed if equation 3.6 (normalized difference snow index) is used, whereas an image with a full snow cover is also needed if equation 3.5 is used.

After a look at potential winter VGT images, the winter image that appeared to be the best from those available was taken on February 8, 1999. This does not mean that this image can be considered as an optimal full snow cover reference image. The snow cover was relatively shallow in 1999, except for a few weeks in March during which clouds have prevented the acquisition of a winter image with a sufficiently deep snowpack. A shallow snow cover means that even low vegetation can contribute to the reflectance of high resolution pixels in open areas. Then, any index based on such an image will be affected.

Table 6.2 Comparison of reflectance values estimated from HRVIR and VGT pixels . Only land use classes in bold are used in figure 6.3

Lande use classe	% of land use occupation	Reflectance								
		B2			B3			B4		
		HRVIR		VGT	HRVIR		VGT	HRVIR		VGT
		Mean %	<i>SD</i>	%	Mean %	<i>SD</i>	%	Mean %	<i>SD</i>	%
Clouds	3.7	24.92	12.1	8.15	35.73	11.31	14.14	25.18	9.22	12.71
Clear water and shadows	2.2	2.50	1.15	7.73	5.24	2.79	12.06	4.66	1.85	9.43
Mixed forest with snow	3.7	13.33	4.74	7.67	22.32	3.47	20.27	13.02	3.17	17
Forest clearing1 With snow	1.7	22.41	8.53	17.50	29.70	6.07	24.27	11.03	3.18	12.14
Frozen water	0.7	12.61	3.8	11.67	10.04	3.11	11.92	4.27	3.23	6.03
<b>Dense deciduous forest</b>	12.9	6.94	1.48	7.08	17.73	2.48	15.64	17.72	3.31	21.09
<b>Low density deciduous forest</b>	5.8	9.44	1.38	8.88	20.47	2.5	16.57	21.95	3.15	21.43
<b>Open areas (1)</b>	12.9	9.72	2.78	9.96	18.82	3.85	13.96	16.40	3.72	18.12
<b>Open areas (2)</b>	5.6	6.55	2.85	7.67	13.12	4.37	16.16	10.11	3.5	19.15
<b>Open areas (3)</b>	7.9	10.32	1.89	8.57	24.04	3.07	20.87	20.00	3.31	23.21
<b>Open areas (4)</b>	10.7	13.88	2.47	12.06	26.92	4.1	22.17	24.83	3.73	22.01
<b>Evergreen forest</b>	16.1	4.36	1.41	4.59	18.66	2.44	16.77	10.00	2.23	14.05
<b>Mixed forest</b>	11.8	6.70	2.15	8.76	20.79	3.02	21.39	13.30	3.77	18.83
Frozen water with snow (1)	0.7	26.37	8.36	7.75	19.92	7.06	19.77	3.18	1.34	0.17
Forest clearing2 With snow	1.4	14.16	8.45	24.15	24.04	5.91	34.39	8.40	1.9	12.06
Clouds and frozen water	0.1	31.59	7.69	33.89	29.80	8.85	31.51	15.19	7.87	72.26
Frozen water with snow (2)	0.1	43.96	7.61	1.30	35.76	6.58	5.12	3.06	1.01	18.23
Low density evergreen forest with snow	2.0	11.53	4.56	23.93	24.25	3.79	21.13	9.07	2.03	0

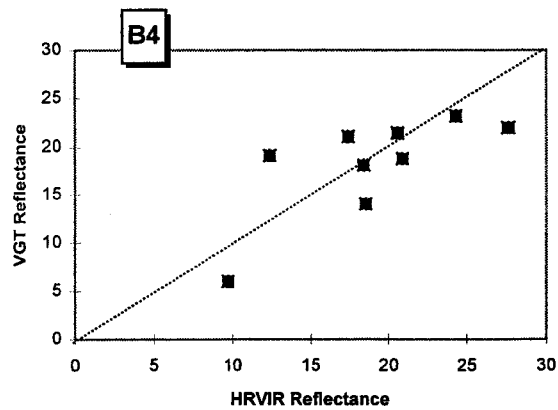
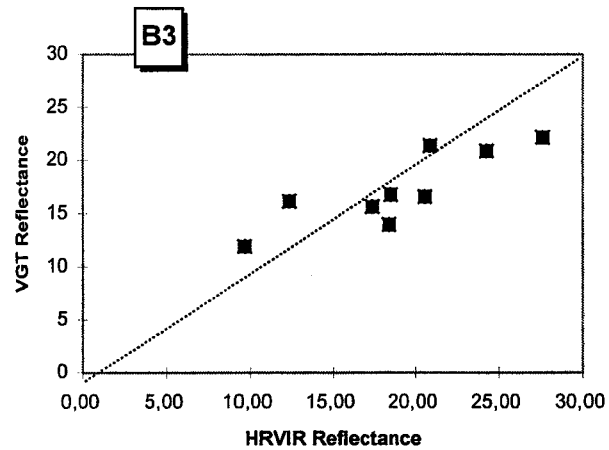
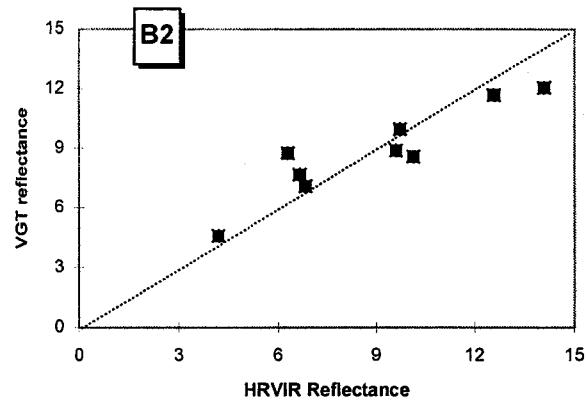


Figure 6.3 Comparison of land use reflectances as estimated from HRVIR and VGT pixels, for the images taken simultaneously on April 11, 1999 and spectral bands B2, B3 and B4.

A VGT image taken at the beginning of May was considered as a good reference image for snowfree conditions over Southern Québec. The selected image was taken on May 2, 1999. Both images are presented in figure 6.4.

For the snowmelt period, it was impossible to take an HRVIR image over the selected region in Southern Québec before April 11, 1999. On that date, most of the snow had melted, but as this was the only available image, we had no choice but to accept it. Finally, we found out that a panchromatic image from the HRV sensor on the SPOT-2 satellite had been taken on April 2, 1999. That image was not from the SPOT-4 satellite and the spectral band was not identical to one of the VGT spectral bands, but at least there was more snow on the ground. So, that image was also purchased. Figure 6.5 shows the VGT and HRVIR images taken on April 11, 1999, whereas figure 6.6 shows the VGT and panchromatic HRV image taken on April 2 1999.

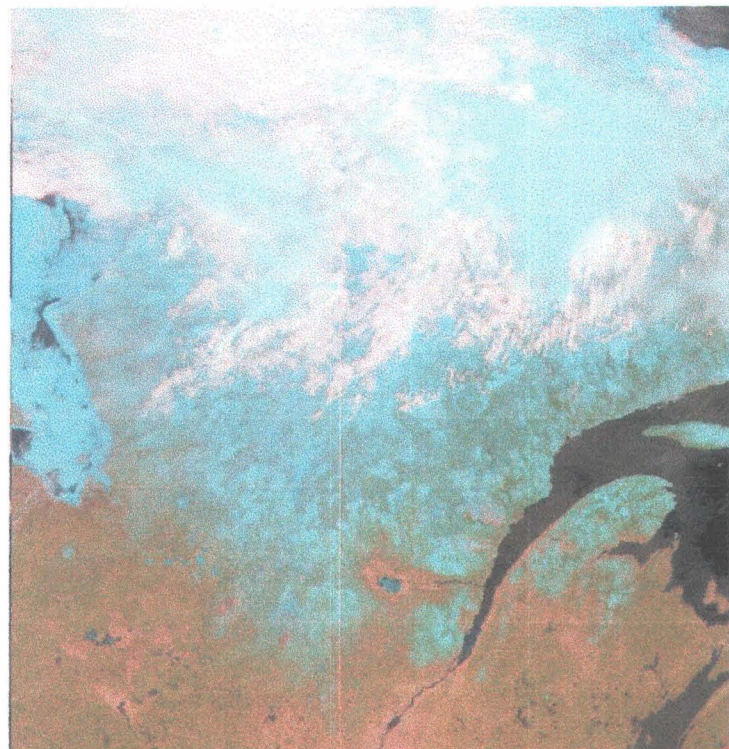
#### **6.4.2 Analysis of the VEGETATION and HRVIR images taken on April 11, 1999**

Considering that the April 11 VGT image was within a few hundred feet from the two VGT reference images (Feb. 8, 1999 and May 2, 1999), we assumed that they could be superimposed accurately. As in the pre-launch phase, we have then estimated the values of  $F$  (equation 3.5) and  $SNDI$  (equation 3.6) and compared those values to the percentage of snow cover as estimated from integration of HRVIR pixels, after determination of the snow covered pixels in the various land use classes. As seen in figure 6.7, the results are not very good. As most of the snow has disappeared, most of the points on figure 6.7a and 6.7b correspond to very low percentages. It is not possible to find out a tendency for higher percentages.

The obvious conclusion to draw from figure 6.7 is that the April 11, 1999 HRVIR image could not be used to verify the results obtained in the pre-launch phase, as far as determining a relation between snow cover as obtained from the VGT pixels image and snow cover as obtained from integration of classified HRVIR pixels on 1000 X 1000m areas corresponding to VGT pixels.

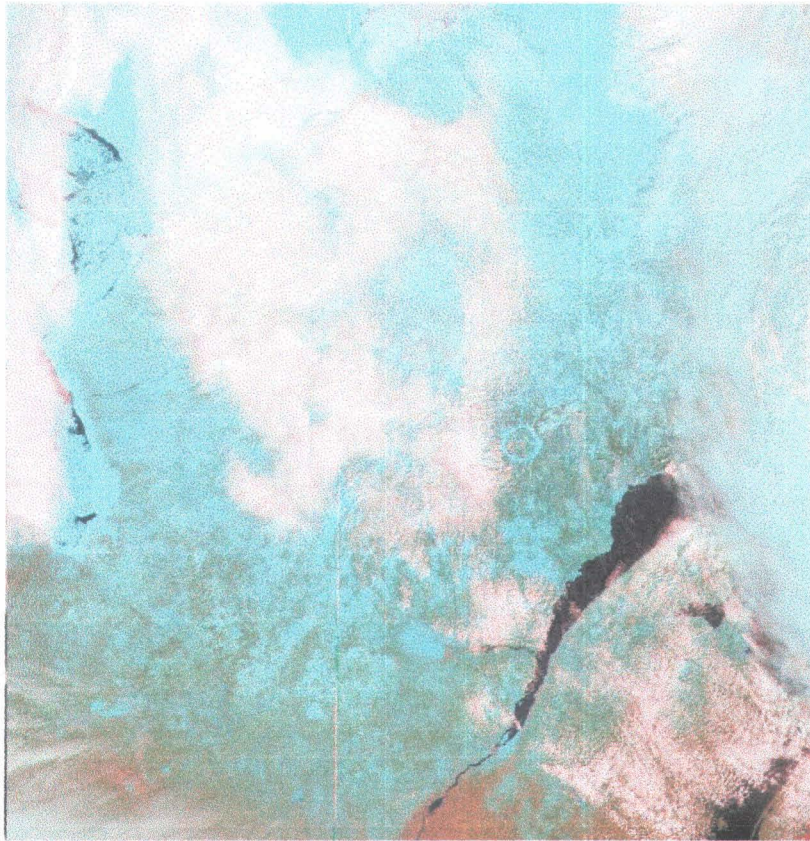


a) February 8, 1999.

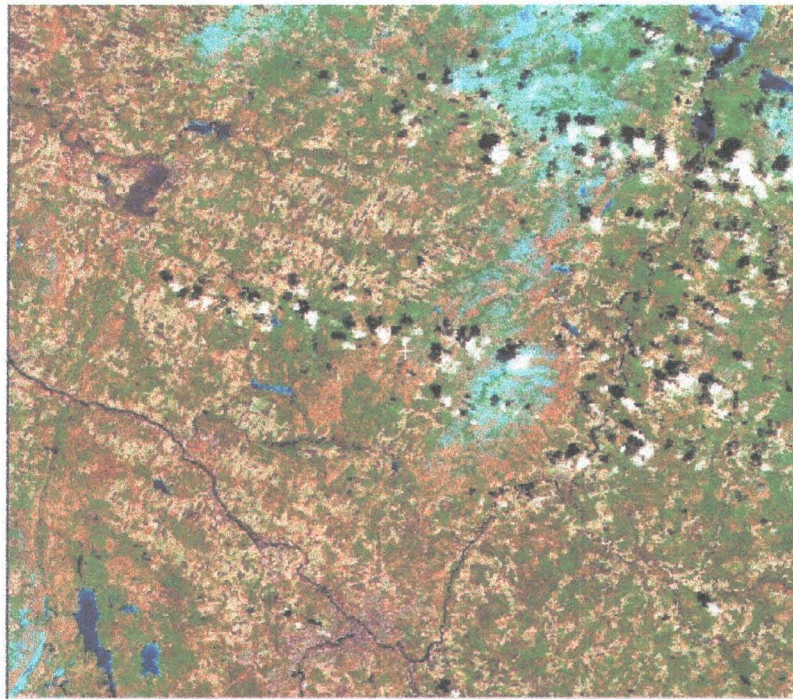


b) May 2, 1999.

Figure 6.4 VGT images used as references

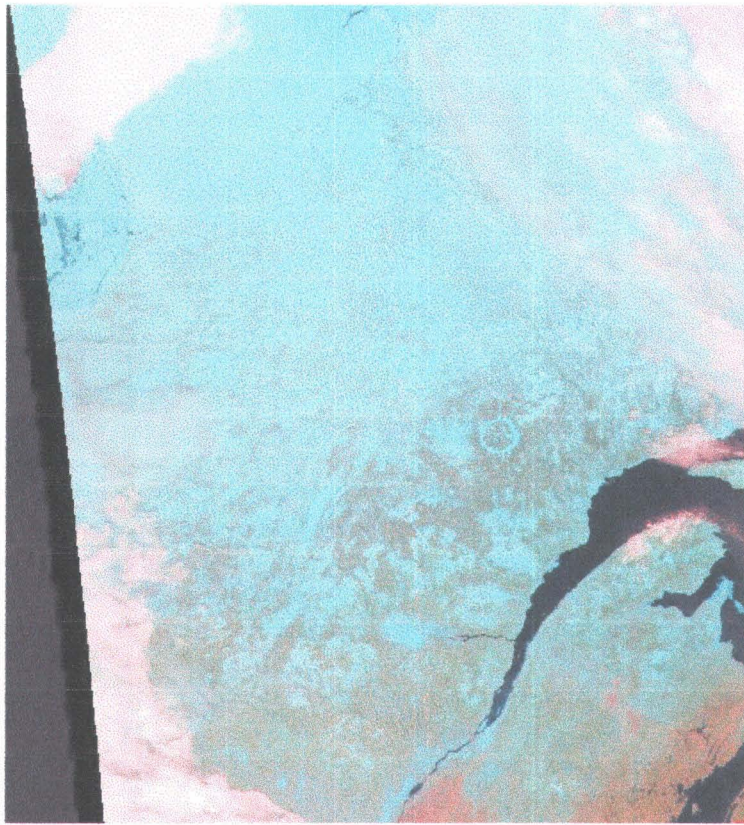


a) VGT image

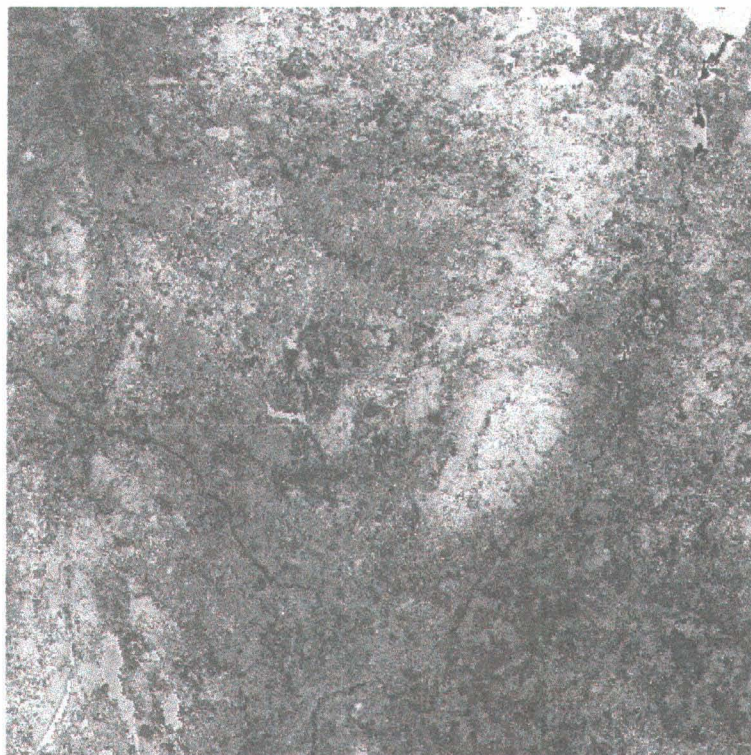


b) HRVIR image

Figure 6.5 HRVIR and VGT images taken simultaneously on April 11, 1999.

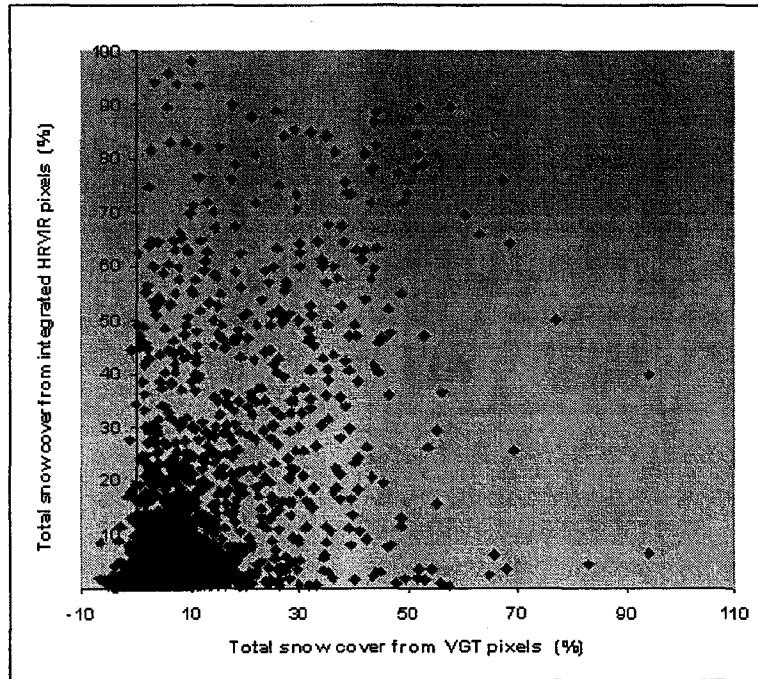


a) VGT image

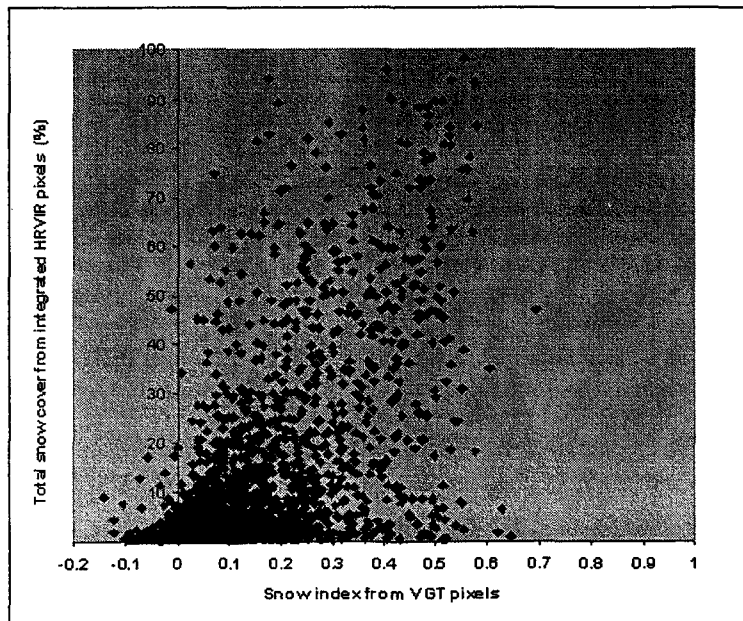


b) HRV image

Figure 6.6 VGT and HRV images taken on April 2, 1999.



- a) Total percentage of snow cover estimated from integrated HRVIR pixels as a function of the total snow cover estimated from VGT pixels (equation 3.5)



- b) Total percentage of snow cover estimated from integrated HRVIR pixels as a function of the normalized difference snow index (NDSI) of equation 3.6.

Figure 6.7 Snow cover estimations with the F and SNDI indices for April 11, 1999 VGT image.

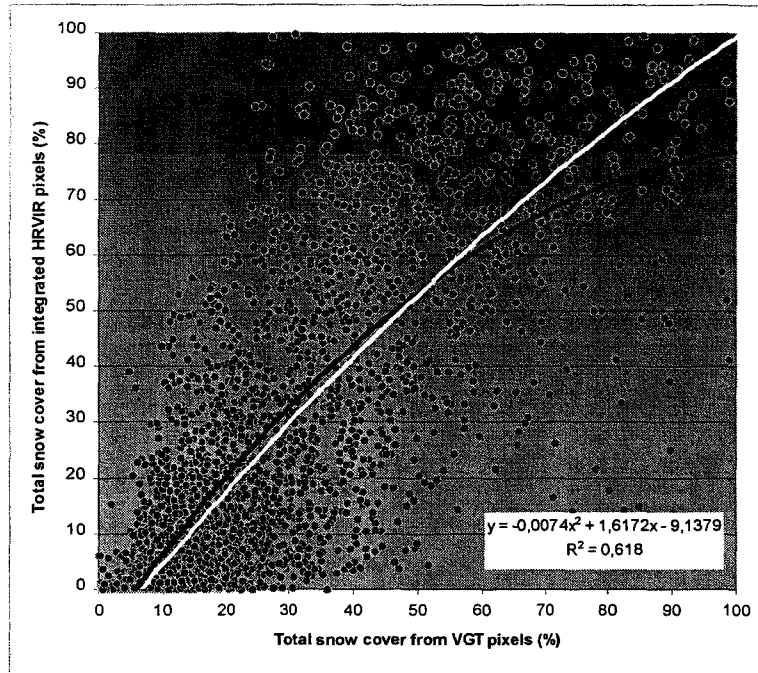
### 6.4.3 Analysis of the VEGETATION and HRV images taken on April 2, 1999

No verification being possible with an HRVIR image taken simultaneously with a VGT image on the same satellite and for the snowmelt period in Southern Québec, we had to turn our hopes to the panchromatic image taken on April 2, 1999 by the SPOT-2 satellite. Again, we have estimated the values of  $F$  (equation 3.5) and SNDI (equation 3.6) and compared those values to the percentage of snow cover as estimated from integration of HRV pixels, after determination of the snow covered pixels in the various land use classes. The results are shown in figure 6.8.

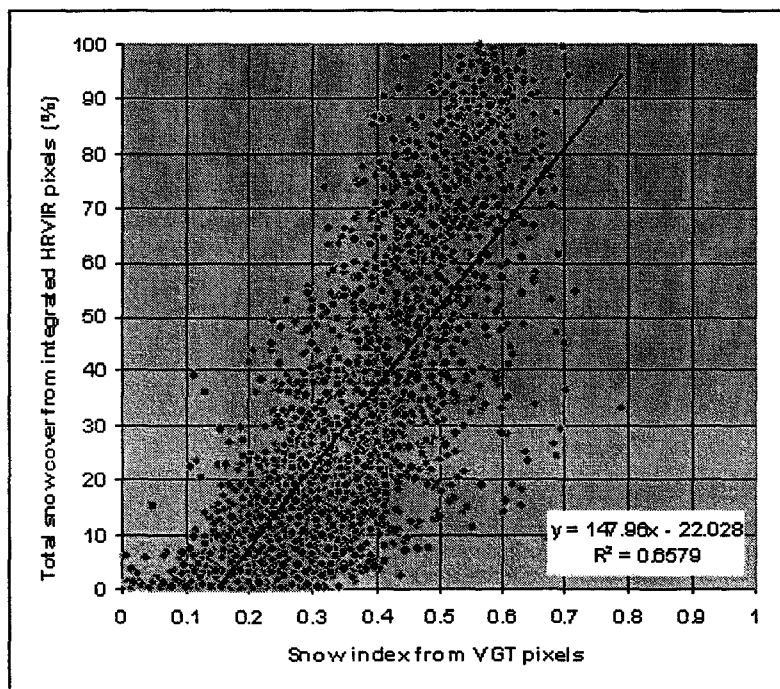
For the relation between the  $F$  value and the percentage of snow cover from integration of HRV pixels (figure 6.8a), again there are more values in the lower percentages, but there are more pixels with higher percentages of snow cover, so that a tendency can be seen. It is not as good as that found out with simulation data (figure 4.3a). In that case, the distribution of points between the various percentages was more regular and there were even more points close to 100%, as the snow covered area was more extensive. As in the simulation case, the relation between total snow cover and  $F$  is not linear. A curve was fit to the data, but of high  $F$  values corresponding to lower snow cover percentages draw the curve downward. Ideally, the curve should go through (0,0) and (100,100), which it does not.

The distribution of point for the SNDI case (figure 6.8b) is similar to that found out with simulated data (figure 4.3b). Again, it should be noted that the density of points becomes greater as the percentage of snow cover decreases. A linear relation can be estimated between the percentage of snow cover on a VGT pixel and the SNDI value, as in the pre-launch phase. Again, points with larger SNDI values corresponding to relatively low snow cover percentages draw the relation downward. It is worth nothing that the slope of the linear relation is relatively close to that obtained previously, but it is shifted towards the right.

More information can be obtained from the HRV image, concerning the percentages of snow cover in various land use classes and the total snow cover on the area corresponding to a VGT pixel. Each value on the four graphs of figure 6.9 has been obtained by integration of HRV pixels. As an example, in figure 6.9a the total snow cover on the area corresponding to a VGT pixel comes from the number of HRV pixels covered with snow, no matter what land use class, over the total number of HRV pixels in the same area, e.g. 2500, whereas the total snow cover in open areas is the total number of snow covered pixels in open areas over the total number of HRV pixels in a VGT pixel.

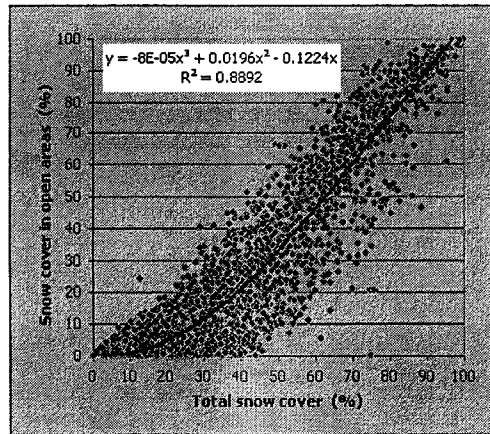


- a) Total percentage of snow cover estimated from integrated HRVIR pixels as a function of the total snow cover estimated from VGT pixels (equation 3.5). The modified relation used to estimate snow cover percentage in figure 6.10c is added. It is the following:  $y = -0.0031 F^2 + 1.394 F - 9.1278$ .

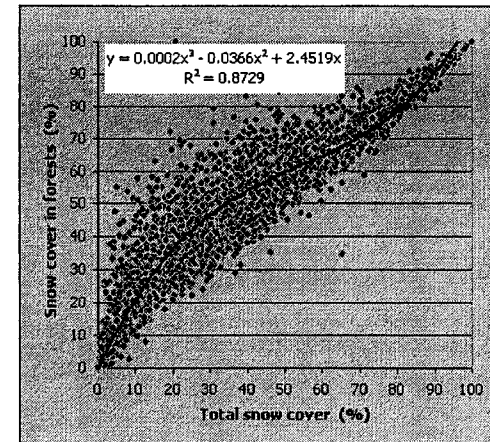


- b) Total percentage of snow cover estimated from integrated HRVIR pixels as a function of the normalized difference snow index (NDSI) of equation 3.6.

Figure 6.8 Snow cover estimations with the F and SNDI indices for the April 2, 1999 VGT image

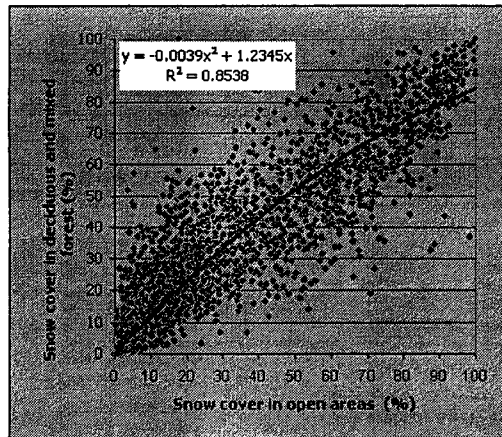


April 2, 1999

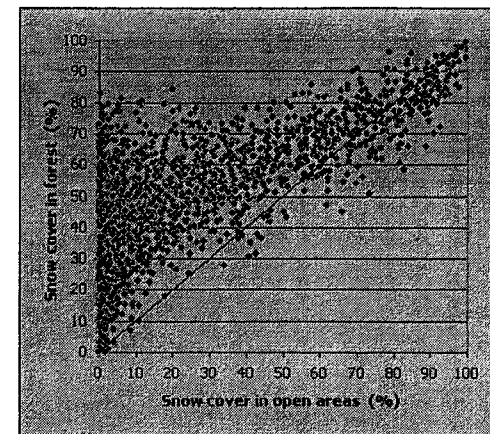


- a) Percentage of open areas covered by snow on each area corresponding to a VGT pixel as a function of the total area covered by snow on that pixel. Both values are from integration of HRVIR pixels.

- b) Percentage of forested areas (deciduous and coniferous) covered by snow on each area corresponding to a VGT pixel as a function of the total area covered by snow on that pixel. Both values are from integration of HRVIR pixels.



- c) Percentage of deciduous and mixed forests covered by snow on each area corresponding to a VGT pixel as a function of open areas covered by snow on that pixel. Both values are from integration of HRVIR pixels.



- d) Percentage of forested areas (deciduous and coniferous) covered with snow on each VGT pixel as a function of open areas covered with that pixel.

Figure 6.9 Snow cover estimation for various land use classes using integration of HRV pixels on areas corresponding to VGT pixels. (April 2, 1999).



The relations obtained with simulated data (figure 4.3 b and c) gave relatively good results in agreement with what could be expected from the physics of snowmelt processes in various land use classes. In short, snow melts more rapidly in open areas than in forested areas. Then, for a given percentage of snow cover in a VGT pixel, we should find a lower percentage of snow in open areas. This is what we observe in figure 4.3c. Also, if the percentage of snow in deciduous forest is compared to that in open areas, it can be seen that the percentage of snow cover in open areas diminishes to less than 50% before there is significant melt in forested areas. Melting occurs even later in evergreen forests.

Let us now look at figure 6.9. In figure 6.9a, we have the total snow cover in open areas as compared to the total snow cover on the same VGT pixel. It can be seen that the percentage of snow in open areas is lower than the total snow cover on the pixel, in agreement with our pre-launch results (figure 4.3c). The points are more spread around the curve than in figure 4.3c and there are less points for higher snow cover percentages as mentioned previously. The total snow cover in forested areas (both deciduous and evergreen forests), on the contrary, is higher than the total snow cover on the same VGT pixel, also as expected. Figure 6.9c is similar to figure 4.3d, but mixed forests have been added to deciduous forests. In that case, the relation between snow cover in forested areas and snow cover in open areas shows more similar percentages. The reason why it does not behave like in figure 4.3d is not clear as we are in the same region. One possible reason could be that we are later in the melt period. Finally, in figure 6.9d, evergreen forests are added to the other types of forested areas. As snow melts more slowly in evergreen forests, it is not surprising to find out a number of percentages over 50% in forested areas, whereas snow has completely melted in open areas.

#### **6.4.4 Mapping of the snow cover at the sub-pixel level**

Even if it was not the ideal reference high resolution image that we would have liked, the panchromatic image taken on April 2, 1999 allowed us to find out results sufficiently similar to those that we had obtained with simulation data to consider that we could try mapping the snow cover at the sub-pixel level. Let us look at the spatial distribution of snow cover at the sub-pixel level as estimated from VGT pixels for both April 2 and April 11, 1999.

Figure 6.10 shows the distribution of snow cover at the sub-pixel level on April 2, 1999. The areal distribution of snow cover percentages on 1000m x 1000m areas corresponding to VGT pixels, as estimated from integration of HRV snow covered pixels is first shown in figure 6.10a. It should be considered as the objective to reach with application of the spectral mixture theory to the VGT

image taken on the same day. Snowfree pixels are clearly identified in the southern portion of the image. The highest percentages of snow can be observed over the Stokes mountains in the eastern half of the image. Figure 6.b shows the areal distribution of snow cover as estimated from the F value (equation 3.5). It can be observed that the snow cover pattern is relatively well reproduced, with a tendency to underestimate the highest percentages and overestimate the lowest percentages. It should be remembered here that the relation between the F value and the total snow cover on a VGT pixel is not linear as shown in figures 4.3a and 6.8a. Application of the relation determined from the April 2, 1999 data on figure 6.8a lead to underestimation of the highest snow cover percentages as the maximum percentage estimated with that relation is 80%. So, it was considered that we should not use that relation without modification. The relation estimated from the April 2, 1988 data in figure 4.3a lead to results that had a tendency to overestimate the percentages, so we have modified the relation on figure 6.8a by staying relatively close to the original curve for values of F smaller than 50% but selecting points higher than the original curve for values of F higher than 50%, so that to reach percentage values closer than 100% as the value of F became closer and closer to 100%. The result is shown in figure 6.10c. The highest snow cover percentages are estimated with a better accuracy. The difference in snow cover percentages for each VGT pixel is shown in figure 6.10d. It is seen that for 55.9% of VGT pixels the estimation lies within  $\pm 10\%$  of the percentage estimated from HRV snow covered pixels. We have overestimation between 10 and 25% for 16% of the pixels and underestimation between -10 and -25% for 14.6% of the pixels.

Then, 86.5% of the estimations from VGT pixels are within  $\pm 25\%$  from the estimations made from HRV pixels, which is quite good, if one considers that otherwise he could only decide that a VGT pixel is snow covered or not.

Nine day later, on the 11th of April, there was much less snow on the ground. As shown in figure 6.7a, it was impossible to even try to find out a relation between the F values and the percentages of snow cover from HRVIR pixels. That did not mean that it would be impossible to map the snow cover at the sub-pixel level. Figure 6.11a presents the areal percentage of snow cover as estimated by integration of snow covered HRVIR pixels. It is the reference image. It can be seen that there is much less snow than on April 2, 1999. Snow cover is mainly concentrated over the Stokes mountains and over the higher elevations to the north of the mountains. Figure 6.11b corresponds to the areal distribution of F values, whereas figure 6.11c is obtained using the same relation between the F value and the percentage of snow cover estimated from snow covered HRVIR pixels as used for the April 2, 1999 VGT image. In both figures, as a negative snow cover is impossible and

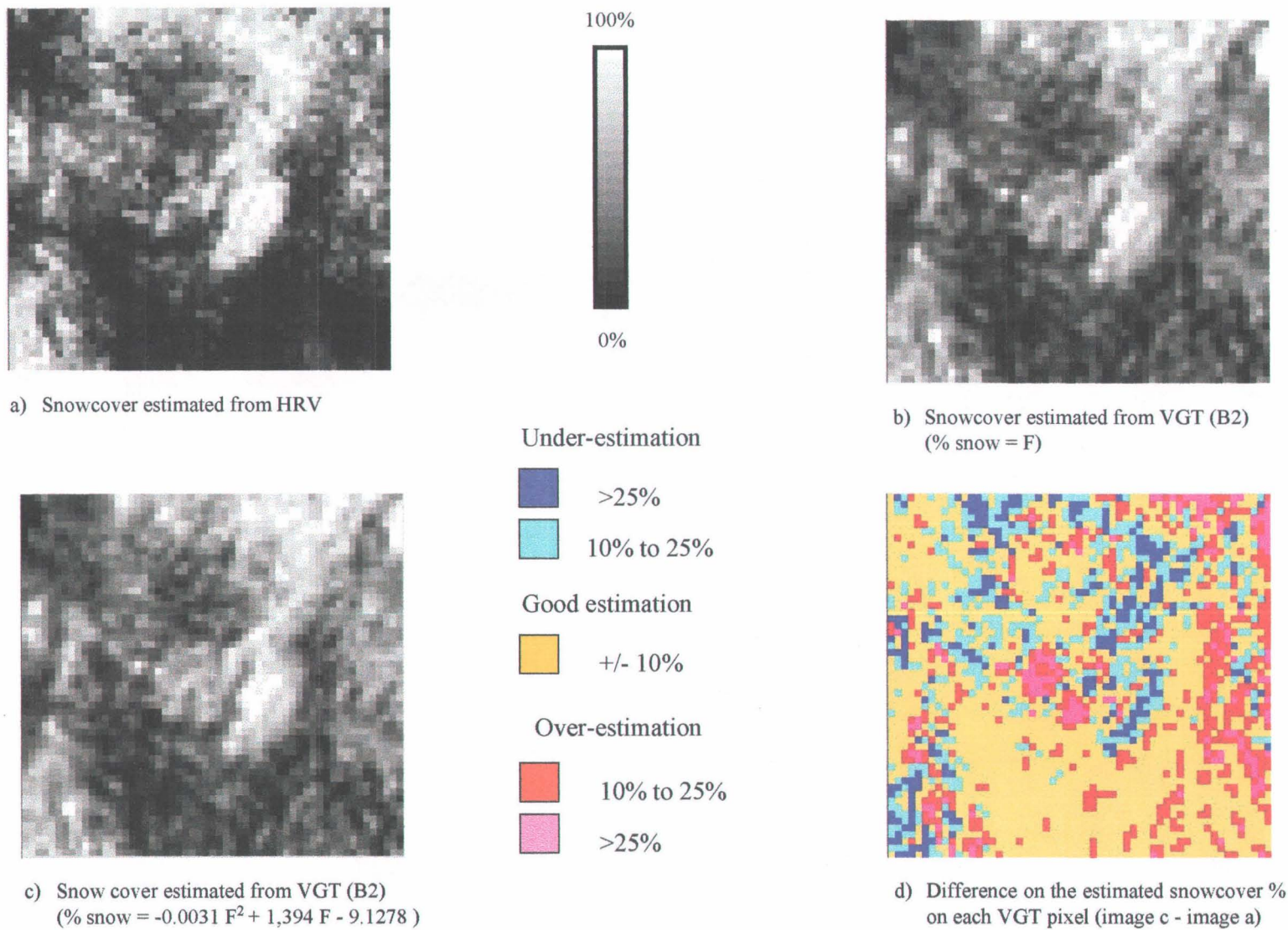


Figure 6.10 Snow cover distribution at the sub-pixel level on April 2, 1999.

negative F values can be obtained for pixels for which the reflectances of snowfree surfaces on the partial snow cover image is lower than the reflectances of the same surface for the snowfree image taken in Fall or Spring, all values of F smaller than zero have been assumed to equal zero. Estimation of the areal distribution of snow cover is very good, as for 80.6% of the pixels, it is within  $\pm 10\%$  of the percentage estimated from integration of snow covered HRVIR pixels (figure 6.11d). We have over-estimation between 10 and 25% for 2.8% of the pixels and underestimation between -10 and -25% for 9.1% of the pixels. Then, 92.5% of the estimations from VGT pixels are within  $\pm 25$  from the estimations made from HRV pixels.

#### **6.4.5 Mapping of the snow cover at the sub-pixel level for a larger area in Southern Québec**

The objective being to monitor snowmelt in regions including at least a few watersheds in order to use the information on snow cover at the sub-pixel level for snow cover updating in an hydrological model, we have applied for the same dates the procedure used in 6.4.4 to a larger area including a number of watersheds in Southern Québec. The results are presented in figures 6.12 and 6.13. In can be noticed in figures 6.12a and 6.13a, that from the 2nd to the 11th of April the snowfree area has progressed in a northeasterly direction, leaving only the areas in higher elevations still covered with snow. North of the St. Lawrence river the snow cover remains predominant. It could be possible to classify figures 6.12a and 6.13a to obtain a snow cover map. That would only give the information that a VGT pixel is covered or not covered with snow. That would already be a valuable information. However, application of the procedure used in 6.4.4 furnishes even more valuable information. Figures 6.12b and 6.13b show indeed that a more detailed snow map can be produced. The percentages are grouped into classes for better visual discrimination in the figure, but individual percentages for each VGT pixels are available as shown previously in the preceding figures. These percentages could still be extended to get an estimation of the snow cover in open areas, deciduous and evergreen forests and use that information to update an hydrological model.

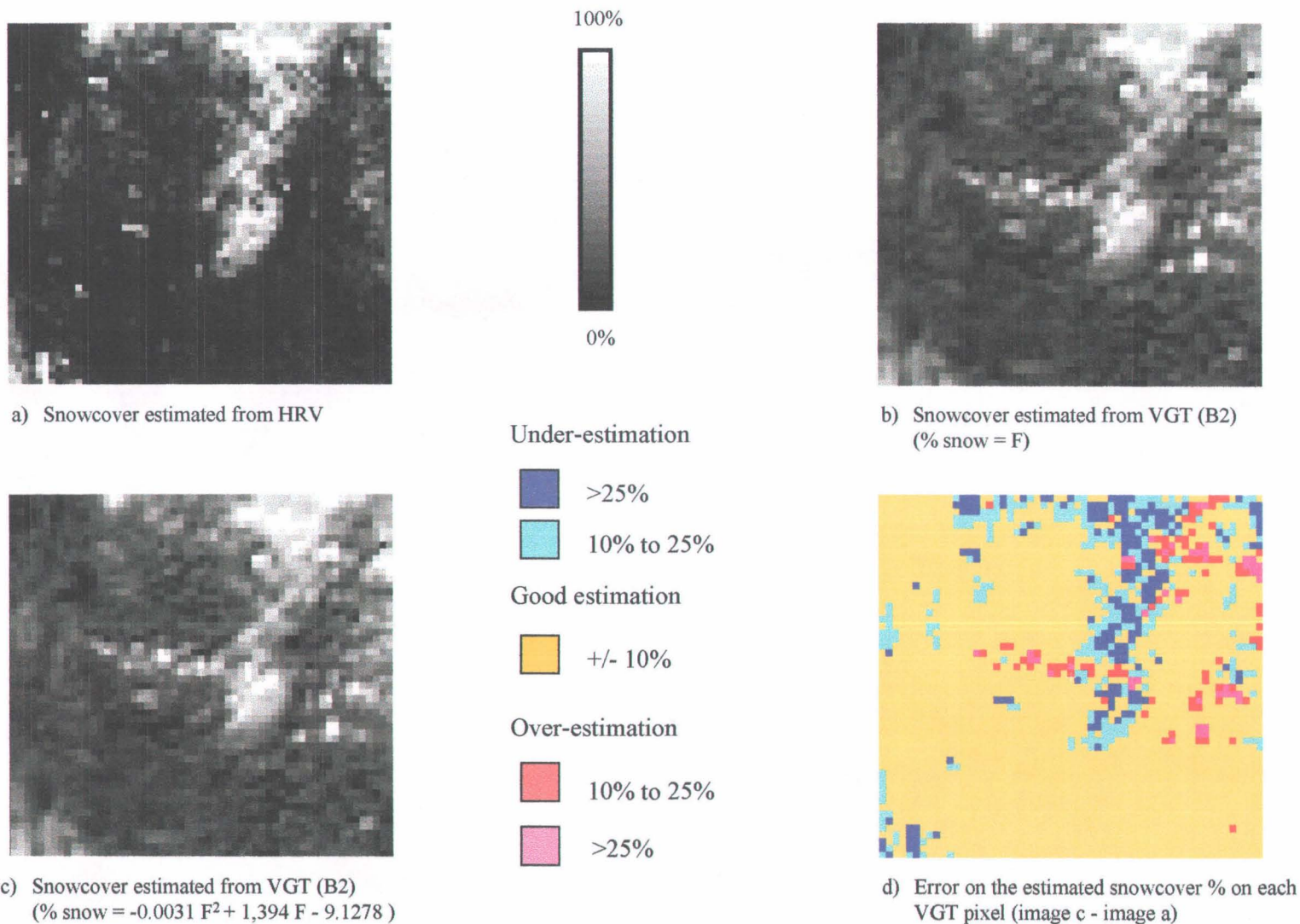
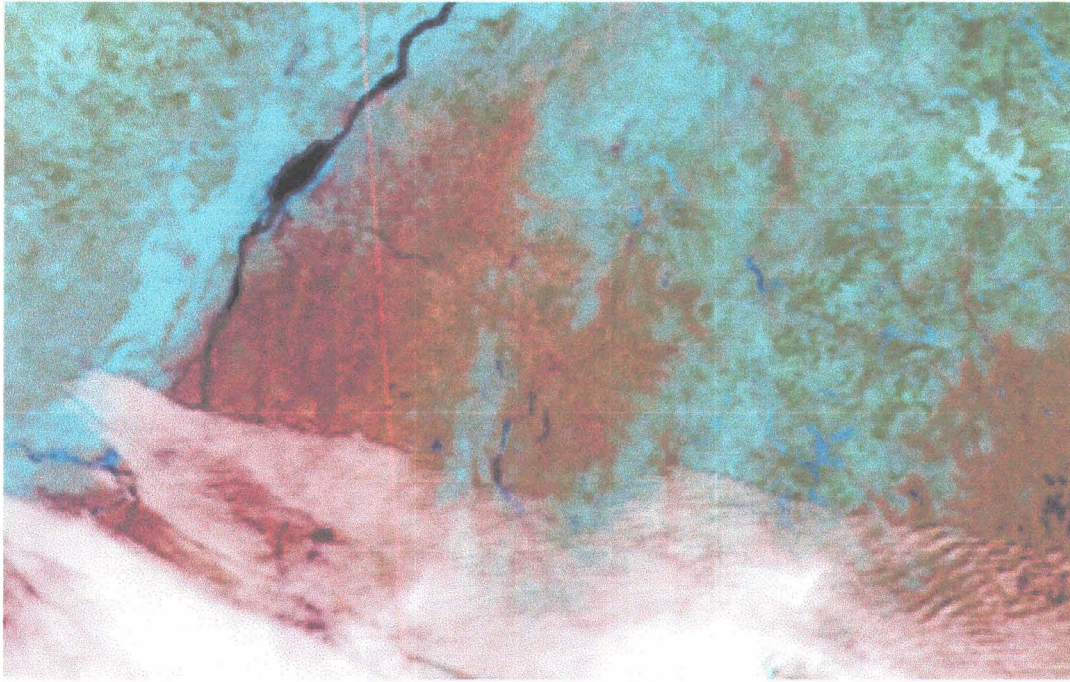
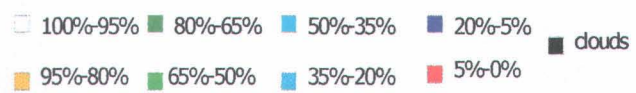
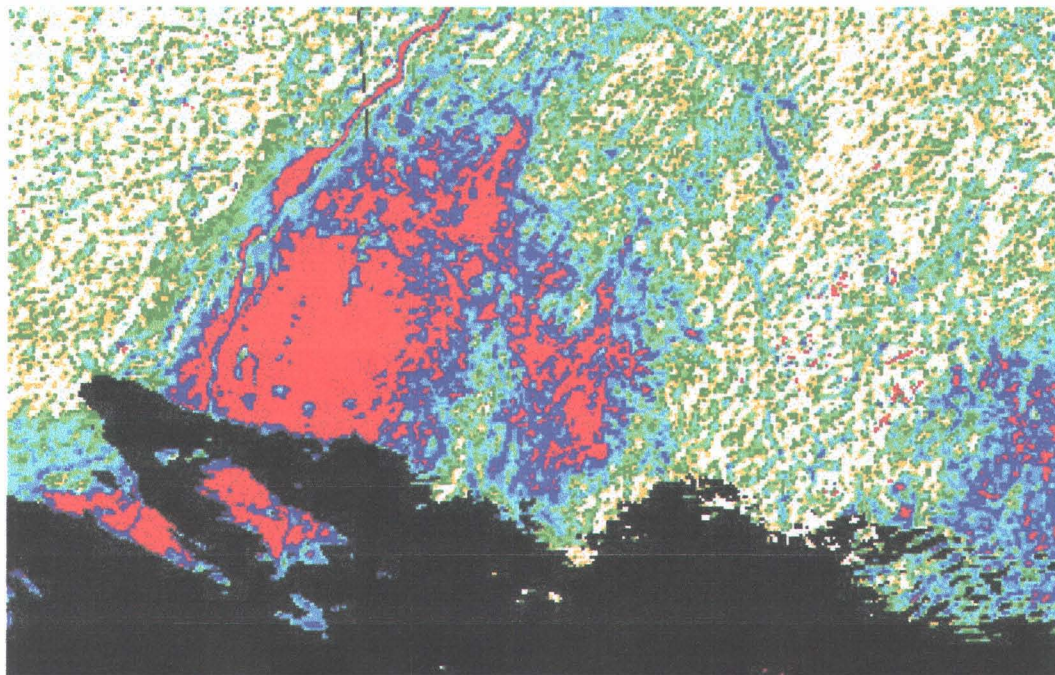


Figure 6.11 Snow cover distribution at the sub-pixel level on April 11, 1999.

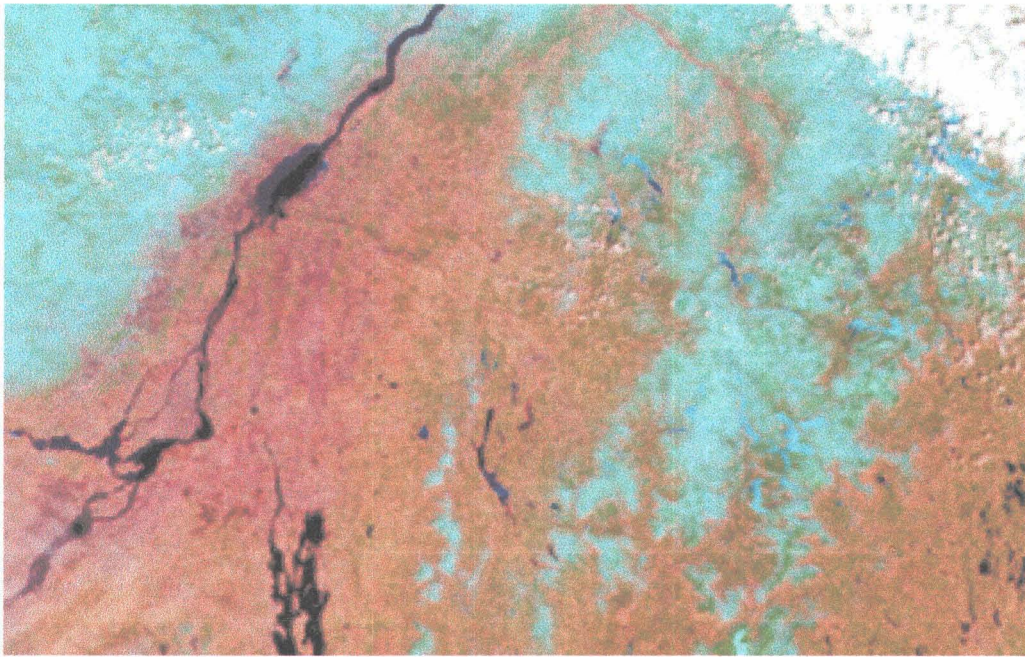


a) False color VGT image. B2 in blue, B3 in green and B4 in red.

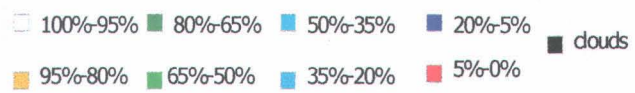
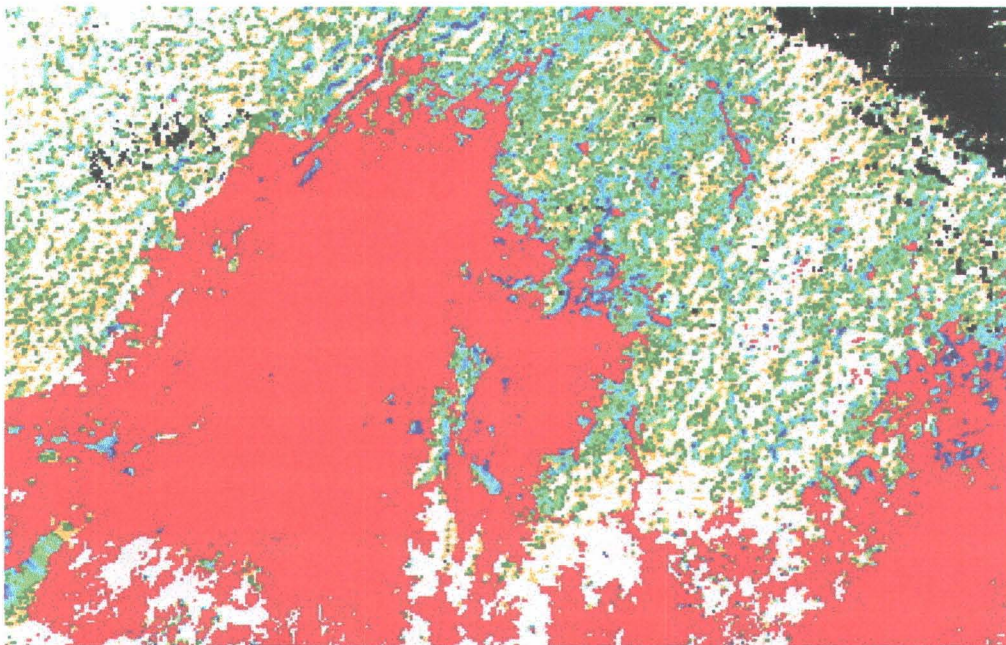


b) Snow cover mapping (%).

Figure 6.12 Snow cover distribution at the sub-pixel level in Southern Quebec on the 2<sup>nd</sup> of April, 1999.



a) False color VGT image. B2 in blue, B3 in green and B4 in red.



b) Snow cover mapping (%).

Figure 6.13 Snow cover distribution at the sub-pixel level in Southern Quebec on the 11<sup>th</sup> of April, 1999.



## 7 DISCUSSION

---

After having obtained very promising results with simulated VGT and HRVIR data, we were hoping to get even better results with the actual data. Unfortunately, it was impossible to make the acquisition of a HRVIR reference image at the right time at the right spot. However, the HRVIR image taken on the 11th of April, 1999 has allowed us to verify successfully our procedure for the estimation of the multispectral and multitemporal registration of VGT images as well as their collocation with an HRVIR image. Estimation from VGT images, of the mean reflectances of land use classes present on the area covered by the HRVIR image on April 11, 1999 was also relatively good. In order to meet, at least partially, the other objective bearing on the estimation of snow cover at the sub-pixel level, we had to use a panchromatic image taken on April 2, 1999 by the SPOT-2 satellite. Even if the snow cover was more extensive than on April 11, 1999, it was not as extensive as in the image used for the simulation in the pre-launch phase, with the result that the curves previously obtained could not be reproduced as accurately as we would have liked. The tendencies are there, but we had to use a curve a little different from the one that had been determined in the pre-launch phase (see figure 4.3). For the moment, we cannot consider either of them as the curve to use for other applications. This does mean that the results are bad. Let us remember that in section 6.4.4 and for the 11th of April, 1999, we have estimated the areal distribution of snow cover within  $\pm 10\%$  of the percentage estimated from integration of snow covered HRVIR pixels (figure 6.11d) for 80.6% of the pixels. If the equation in figure 4.3 is used that percentage falls only to 75.5%. Also the equation used in the pre-launch phase has a greater tendency to overestimate the snow cover than the equation derived from the April 2, 1999 data (11.6% against 2.8%), but underestimation is much better (4.2% against 9.1%). Then, whereas 92.5% of the estimations from VGT pixels are within  $\pm 25\%$  from the estimations made from HRV pixels for the equation derived from the April 2, 1999 data, that percentage was 91.3 for the equation derived from the pre-launch data. Both results are quite good, but further estimations using other data sets would help to determine relations that could be used operationally with confidence.



## 8 CONCLUSION

---

For the post-launch phase we were not able to obtain the proper synchronisation between snowmelt processes in the primary region of interest and acquisition of high resolution HRVIR data. As a result, whereas in the pre-launch phase we could conclude that it was possible to reach our objectives, in the post-launch phase we have only been able to conclude that those objectives could most probably be reached with a better set of data as far as the estimation of the percentage of snow cover on each VGT pixels is concerned. The other objectives have been met.

During the next months, we will continue to work on the VGT images already obtained to try and understand if we can get more precise information from them. We will also apply them to areas north of the St. Lawrence river, as monitoring snowmelt in those regions on a day-to-day basis, even using a relation that could be more accurate, would still give an information on snow cover that cannot be known otherwise from ground data.



## BIBLIOGRAPHY

---

Kerdiles, H. and M.O. Grondona (1995). NOAA-AVHRR NDVI decomposition and subpixel classification using linear mixing in the Argentinean Pampa. *Int. J. Remote Sensing*, 16(7): 1303-1325.

Novo, E.M. and Y.E. Shimabukuro (1997). Identification and mapping of the Amazon habitats using a mixing model. *Int. J. Remote Sensing*, 18(3): 663-670.

Rahman, H., Dedieu, G. (1994). SMAC: a simplified method for the atmospheric correction of satellite measurements in solar spectrum, *International Journal of Remote Sensing*, Vol.15, No.1, pp. 123-143.

Shimabukuro, Y.E., Carvalho, V.C. and B.F.T. Rudoff (1997). NOAA-AVHRR data processing for the mapping of vegetation cover. *Int. J. Remote Sensing*, 18(3): 671-677.